Multi-Response Design Optimization of Two Axes SU-8 based Scanning Micromirror for Endoscopic Imaging

Author

Fizza Javaid

00000170885

Supervisor

Dr. Muhammad Mubasher Saleem

DEPARTMENT OF MECHATRONICS ENGINEERING

COLLEGE OF ELECTRICAL & MECHANICAL ENGINEERING

NATIONAL UNIVERSITY OF SCIENCES AND TECHNOLOGY

ISLAMABAD

AUGUST, 2019

Multi-Response Design Optimization of Two Axes SU-8 based Scanning Micromirror for Endoscopic Imaging

Author

FIZZA JAVAID

00000170885

A thesis submitted in partial fulfillment of the requirements for the degree of

MS Mechatronics Engineering

Thesis Supervisor:

DR. MUHAMMAD MUBASHER SALEEM

Thesis Supervisor's Signature: _____

DEPARTMENT OF MECHATRONICS ENGINEERING

COLLEGE OF ELECTRICAL & MECHANICAL ENGINEERING

NATIONAL UNIVERSITY OF SCIENCES AND TECHNOLOGY, ISLAMABAD

AUGUST, 2019

Declaration

I certify that this research work titled "*Multi-Response Design Optimization of Two Axes SU-8 based Scanning Micromirror for Endoscopic Imaging"* is my own work. The work has not been presented elsewhere for assessment. I have properly acknowledged / referred the material that has been used from other sources.

Signature of Student

Fizza Javaid

00000170885

Language Correctness Certificate

This thesis has been read by an English expert and is free of typing, syntax, semantic, grammatical and spelling mistakes. Thesis is also according to the format given by the university.

Signature of Student

Fizza Javaid

00000170885

Signature of Supervisor

Copyright Statement

- Copyright in text of this thesis rests with the student author. Copies (by any process) either in full, or of extracts, may be made only in accordance with instructions given by the author and lodged in the Library of NUST College of E & ME. Details may be obtained by the Librarian. This page must form part of any such copies made. Further copies (by any process) may not be made without the permission (in writing) of the author.
- The ownership of any intellectual property rights which may be described in this thesis is vested in NUST College of E & ME, subject to any prior agreement to the contrary, and may not be made available for use by third parties without the written permission of the College of E & ME, which will prescribe the terms and conditions of any such agreement.
- Further information on the conditions under which disclosures and exploitation may take place is available from the Library of NUST College of E & ME, Rawalpindi.

Acknowledgements

First of all, special blessings of Allah Almighty upon me in my whole journey has extremely gratified me, the ultimate source of acquaintance and knowledge to mankind. Without His blessings upon me, I would never be able to accomplish what I even have achieved till this day.

I would wish to specific sincere feeling to my supervisor Dr. Muhammad Mubasher Saleem for his continuous support, exceptional acument, and constant steerage throughout the course of this thesis.

I wouldn't be here today without his reassurance throughout the final stages of this research.A special thanks to Mr. Muhammad Saqib for his cordial support and for thesis guidance at several stages which helped me in accomplishment of this task timely.

Finally, I would like to express thanks to my family for their support and motivation for me which resulted to be an unceasing source of adoration.

This work is dedicated to my adored parents and beloved siblings who always inspired me to do this great accomplishment

Abstract

The dissertation presents the design of an electrothermally actuated micromirror based on Micro electromechanical system (MEMS) technology. MEMS micromirrors are used in a variety of applications such as projection imaging, optical switching, bar code scanning, microscopic topometry and biomedical imaging like Optical Coherence Tomography. The main emphasis in this effort is to design MEMS scanners for Optical Coherence Tomography with optimum deflection angle. The optimization is based on actuator design, device dimensions and layout using design of experiments techniques. The proposed micromirror device is capable of generating deflection of 0.6 μm at low input power of 1.08 mW. The FEM analysis of the device is simulated in ANSYS.

Key Words: *MEMS, Micromirror, Electrothermal, FEM.*

Table of Contents

List of Figures

List of Tables

Acronyms

MEMS	Microelectromechanical Systems
ETA	Electro Thermal Actuator
RF	Radio Frequency
FEM	Finite Element Method

Chapter 1: Introduction

The research work focuses on the design of MEMS based micro mirrors for integration in Endoscopic Imaging. First, a motivation and scope of this work is briefly discussed. Second, an introduction of MEMS based micro mirrors is described. Third, the prior work in the field of micro mirrors and their actuation techniques is summarized.

1.1 Motivation and Scope

Research has been done to develop the high-resolution optical technology for biomedical imaging in the last few decades. There are many techniques available for biomedical imaging such as X-rays, MRI, Ultrasound, and some of body imaging techniques e.g. terahertz, PET, and Doppler. Optical coherence tomography (OCT) is one of the most demanding imaging technologies due to its high resolution for imaging in turbid and scattered medium like biological tissues. A basic OCT system consists of a Michelson interferometer and depends on backscattered data from scanning and reference arm. In-vivo endoscopic OCT imaging has made the non-invasive imaging technique possible. Early systems use large mechanism like translational stages and external motors to move reference arm or target which limit the speed of scanning due to limitations of these mechanisms. This brings a change to replace the large mechanism with micro level mirrors and scanner. So, micro mirrors played an important role and are used in OCT probe as angular and vertical scanners to scan targets at high speeds. With this increasing demand of MEMS scanners and more optimal bio imaging, there is enough motivation to investigate more optimal and miniature MEMS scanners that are more suitable for OCT and bio imaging applications.

1.2 Introduction to Micromirror

MEMS micromirrors devices are used in optical systems with size range of micrometers for light projection over a variety of reflection angles. We can adjust statically or dynamically, the reflection angle of a micromirror that allow the rotation of mirror surface by an actuation mechanism. The actuation schemes used in micromirrors display diverse results in relations of maximum displacement, device size, actuation power, voltage requirements and fabrication difficulty. Micromirror applications requires an extensive variety of specifications related to performance, so depending upon the application, the actuation approach. Micromirror devices are used in several applications such as optical coherence tomography, endoscopic measurements,

simple scanning for bar codes and as switch in optical networks depending on their structure and actuation technique. A variety of product applications used micromirrors in industries that include microscopic topometry [1], bar code scanning [2], imaging [3], optical switching [4,5], and scanning [6]. Widespread research has also been assumed to improve the performance and scrutinise other applications of MEMS micromirrors.

1.3 Prior Work in Micromirrors

Electrothermal, electrostatic, piezoelectric and electromagnetic are major actuation techniques used in micromirrors. We will concisely discuss all four actuation techniques to investigate application areas and previous research work.

An induced Lorentz force is used in electromagnetically actuated micromirrors to generate mirror rotation. When we fabricate a coil structure under the mirror surface of an external magnet together to the mirror, this force is achieved. When a current is applied through the coil of the mirror, the mirror is forced to rotate as Lorentz force is. The position of magnet and induced coil can also be switched with each other. The electromagnetic micromirror motion can be controlled by controlling the direction of the current and amplitude [7-10].

In applications where we need to achieve Large angular displacements (>15◦) electromagnetic actuators are the best choice, but to achieve these large angular displacements, high currents (>100mA) are usually required [11, 12]. We need relatively larger 'Chip area' which makes this type of micromirrors unsuitable for applications.

A micromirror with electromagnetic reported with 2-DOF [7]. The micromirror dimension is 3.5mm×3.5mm and can attain maximum angle of optical deflection 1.5° with 20mA at 2.2K Hz resonance. The optical scanner can be actuated by an external magnetic field as well by electroplating a copper wire. Eddy current were exploited by Yang et al. on a 2mm×2mm mirror plate with 9mW input power [8].

Yalcinkaya et al. elaborated micromirror with an electromagnetic actuation with a 1.5mm×1.5mm device size [9] with 60° of optical scan. An example of electromagnetic micromirror is given by figure 1.1.

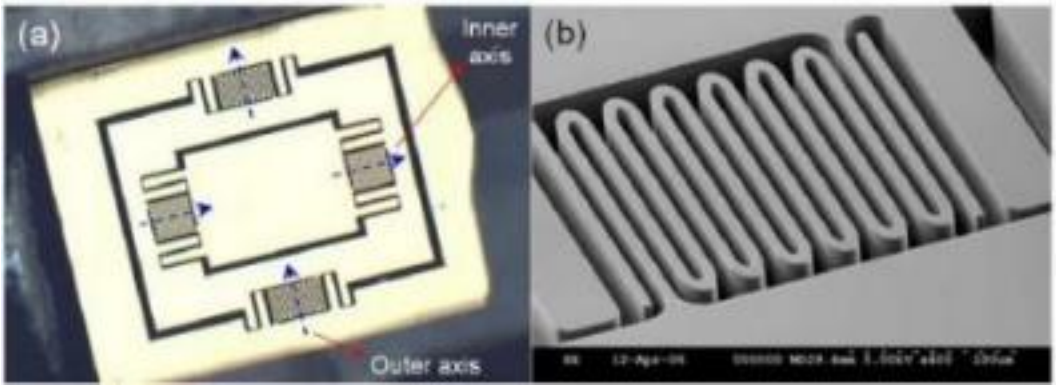

Figure 1.1: Schematic diagram of Electromagnetic (a) SEM picture of a supporting folded flexure. (b) A micro-mirror is supported by a 2-axis gimbal structure composed of folded flexure hinges and can deflect in two orthogonal axes: inner and outer axis depicted in the picture [10].

Piezoelectric actuated micromirrors work when by applying a voltage to a piezoelectric material the force and displacement is induced on it. Piezoelectric micromirrors are typically actuated by rotating the mirror plate using a piezoelectric bimorph that can be used in a different topology [11, 12]. A 1-DOF piezoelectric micromirror is considered by Park et al with a hinged device structure [11]. Aerosol deposition method reports the PZT film preparation on a stainless-steel substrate. An optical scan angle of 40° of has been realised with 60V driving signal at resonance. A micromirror with piezoelectric actuation mechanism reported with a 2-DOF [12]. Its cataracts in a twisting shape cantilever PZT morphs to achieve displacement in angles. The device gives angle of rotation ±8° with fewer than 20V. Piezoelectric micromirrors have been used in projectors [13] and for the optical switches [13]. Larges paces and the layout size of micromirror is not required in this type of design of micromirror as similar to that of an electrothermal design. A significant hysteresis effect is reported in theses designs [12, 13]. Moreover, the use of non-standard materials is essential for the fabrication of the actuators. An example of piezoelectric micromirror is shown in figure 1.2 [14].

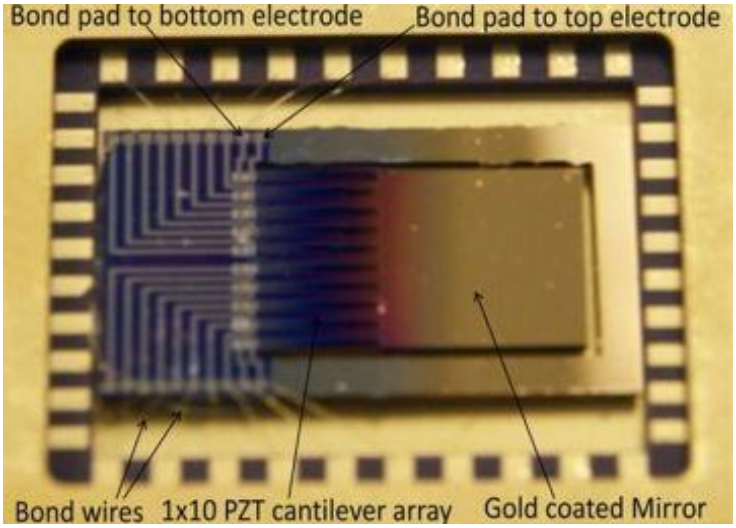

Figure 1.2: Schematic diagram of Piezoelectric [14].

A Columbic force between two oppositely charged surfaces to actuate and Electrostatic micromirror. When a voltage is applied across them, these surfaces which are typically electrodes made of metal or semiconductors, pull in towards each other. This pull-in creates a displacement that can be used in a variety of ways to create mirror surface rotation like levers and torsional beams [12, 15, 16]. A SOI-based angular is reported by Patterson et al. with a vertical comb driven (AVCD) micromirror by making use of photoresist reflow process to generate the moving combs initial tilting [15]. An optical scan angle of 18° is generated at resonance with driving voltage of 100V .A Post-CMOS micromirror is reported by Xie et al. using a multiple metal-oxide layers initial tilt mechanism of stress induced on the CMOS chip and attained a ±4.7° rotation angle at 20V [16].

Electrostatic micromirrors, at comparable voltages, generally results in lower displacements as compared to their counterpart of different design. Deflections of as much as 2◦ at 50–70V[17]. As reported by Zara and Smith, electrostatic actuation leads to large rotation angles (>15◦), resulting high voltages are desirable for this purpose. The advantage of electrostatic actuation is it scans a large area at a short interval of time as its very fast response time. But it cannot be used high voltage sensitive devices due to high voltage requirements. An example of electrostatic micromirror is shown in figure 1.3 [18].

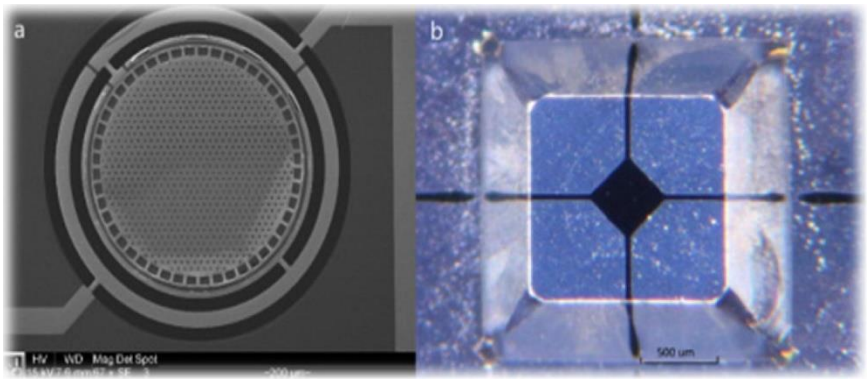

Figure 1.3: Schematic diagram of electrostatic micromirror [15].

Materials typically expand and shrink when their temperature increases or decreases respectively is the basic electrothermal principle. A thermal bi-layer beam structure as actuator in mostly electrothermal designs. A thermal bi-layer actuator is a structure of two material layers bonded at lengths with a significant difference in their coefficients of thermal expansion (CTE). When a change in temperature is applied, it causes the actuator to bend to a side that the material has less value of CTE. The displacement caused is used to rotate the mirror surface. The actuators have the micromirror attached at one end to them.

Electrothermal designs, in comparison to the others, are easy to fabricate and can make use of widely used micro fabrication materials. They also don't require higher currents and voltages as compared to electromagnetic and electrostatic designs respectively. It is important to make sure that the high temperature from the actuator must not affect its application, an application such as micromirror. Careful design and implementation of electrothermal actuators can easily overcome this obstacle in a MEMS device Earlier Ataka and Buhler et al. [19] demonstrated work in electrothermal design. There are many designs with this actuation mechanism reported [20]. Many electrothermal designs for use in optical tomography (OCT) were reported by Xie et al. [16, 21].

Jain et al. reported up to ±30° scanning optical angle with 1-DOF and 2-DOF Also, a SiO2 /Doped Silicon bimorph actuator an electrothermal micromirror also with 16° optical deflection [23].

A precise tracking positioner is stated by Yang et al. made of SiO2 /Doped Silicon materials bimorph actuator [24]. A bimorph actuator is reported by Ataka et al. founded on two layer polyimide material for micro-motion systems [25]. When a change in temperature is applied, it causes the actuator to bend to a side that the material has less value of CTE .This is further cleared by Buhler .He first reported a micromirror with CMOS having bilayer structural layers

of Al/SiO2 with CTE actuation [19]. A more favourable electrothermal bimorph material combination is Al/Polysilicon. Izhar et al. presented an actuator of same combination [26]. He reported an angular displacement of 32° with having and application of 6V and input power of 12mw. Ali et al. also represented a micromirror based on Al/Polysilicon based bimorph actuator [27]. He reported an angular displacement of 38° on application of voltage of 1.3v and input power 9.4 mw. Recently Zhang et al. [28] reported a MEMS scanner electrothermally actuated that can scan a large piston range of up to 800 um at applies voltage of 6V. An example of electrothermal actuator is presented in fig 1.4 [18].

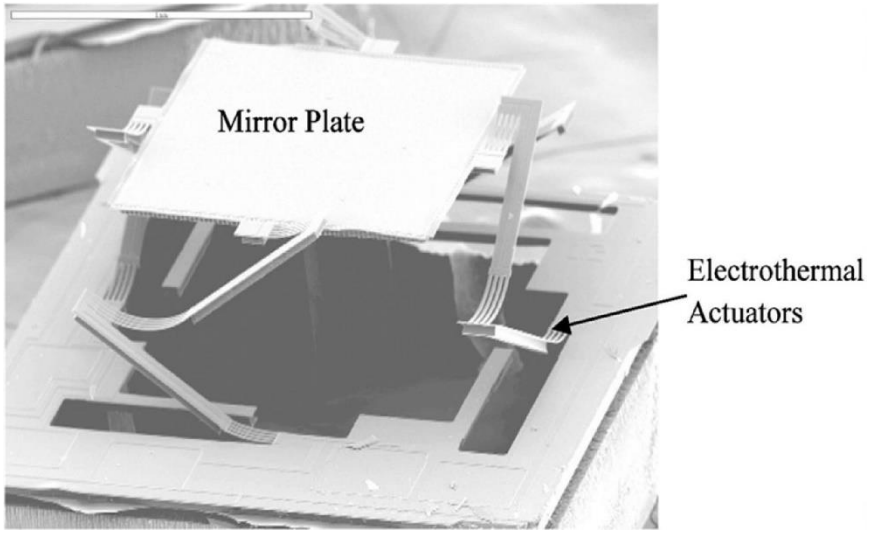

Figure 1.4: Schematic diagram of electrothermal actuated micromirror [18].

A comparison of different actuation techniques is presented in Table 1. It is clear that electrothermal actuation is most suitable for high optical scan range of micromirrors.

Table 1: Comparison of different actuation techniques.

Specifications	**Electromagnetic**	**Piezoelectric**	**Electrostatic**	**Electrothermal**
Deflection	Large	Small	Small	Large
Input Power	High	Low	Low	High
Operating Speed	Fast	High	Fast	Slow
Fabrication Difficulty	Complex	Need exotic materials	Relatively Complex	Simpler
Device size	Large	small	Large	Small

1.4 Microfabrication process

There are various fabrication processes available for fabricating MEMS devices. Processes differ on the basis of material used in fabrication of MEMS device, type of device, feature size and cost**.** MUMPs stands for multi user MEMS process.

1.4.1 SOIMUMPs

SOIMUMPs stands for Silicon on insulator multi user MEMS process. It is one of the most commonly used process for microfabrication. SOIMUMPs based microgrippers have been fabricated previously with both, electrostatic actuators [29] and electrothermal actuators [30] with high power consumption. Due to high strength and low coefficient of thermal expansion of silicon, very low displacements are achieved at very high temperatures. However, high coefficient of thermal conductivity, those high temperatures reach the jaws of microgripper, making it unusable for biomedical application. Material resistivity can be varied using p-type or n-type doping process.

1.4.2 MetalMumps

MetalMumps fabrication process uses metal electroplating to fabricate MEMS device. In this process, Nickel is used as a metal for whole device fabrication. A few microgrippers have been fabricated using this process [31]. However, MetalMumps is not suitable for fabricating microgrippers with biomedical applications, as of high coefficient of thermal conductivity. High temperature can damage the object under manipulation.

1.4.3 PolyMUMPs

PolyMUMPs stands for polysilicon multi user MEMS process. It is a micromachining process commonly used for fabrication of MEMS sensors. It has three layers, of which, two layers are sacrificial and one metal layer. Seven layers can be formed using up to eight masks. Minimum feature size for this process is 2 μm. Very few microgrippers have been fabricated using this process [32]. Material properties of polysilicon differs for silicon. It has also high coefficient of thermal conductivity, and low coefficient of thermal expansion. Microgripper fabricated from this process have high power consumption.

1.4.4 LIGA process

LIGA is another MEMS fabrication technique, usually used to produce various aspect ratio designs and structures. There are two main types of LIGA fabrication technologies, X-ray based and UV based. X-ray based fabrication is used for high aspect ratio designs while UV based fabrication is for low aspect ratio for designs which is more commonly used. This process consists of three main steps: Lithography, electroplating and molding. This technique is used to fabricate a few microgrippers [33].

1.4.5 Polymer based fabrication

For past few decades, many MEMS devices have been fabricated using this process. Commonly used polymer is SU-8. SU-8 is an epoxy based negative photoresist. Negative represents, if is exposed to ultraviolet light, the structure become permanent, while unexposed region remains washable. Multiple layers of SU-8 can be added to increase thickness of structure, which also depends on which variant of SU-8 is used. Minimum feature size is 5 μm, however, feature size below 5 μm has also been achieved using complex processes [34]. Polymer based fabricated microgrippers have been fabricated due to SU-8's biomedical compatibility.

1.4.6 Advantages of SU-8

SU-8 polymer has multiple advantages over silicon, polysilicon and metals. SU-8 has many variants, with slight difference in material properties. Besides low coefficient of thermal conductivity of 0.2 W / (m K), it has high coefficient of thermal explosion of 52×10^{-6} 1/m [35]. In addition, it has high electrical resistivity, which aids in isolating electrical circuit from its mechanical end effector. Low coefficient of thermal conductivity does not let high temperatures to reach to jaws of microgripper. For designing better performing electrothermal actuators, high coefficient of thermal expansion is required which SU-8 has. SU-8 based electrothermal actuators have very low electrical power consumption due to very thin metallic heater. Therefore, we choose SU-8 polymer for design of our microgripper.

Table 2: Material Properties.

Material Properties (Units)/Materials	**SU-8**	**Silicon**
Young's Modulus (GPa)	4.60	162
Poison Ratio	0.22	0.22
Density (Kg/m^3)	1200	2320
Specific Heat (J/ (kg °C))	1674.8	702
Coefficient of Thermal Conductivity (W/ (m °C))	0.2	150
Coefficient of Thermal Expansion (1/ °C)	52×10^{-6}	2.66×10^{-6}

1.5 Introduction to OCT

Optical coherence tomography is an imaging technique which helps to analyse real-time, vivo imaging, non-invasive, with high resolution at micrometres range. The system is capable of high spatial resolution and non-invasive imaging. This is following on basic principle of interference principle and works on interaction between reflected light from target and reference beam [36].

OCT functions for two beams of lights through two arms. The beam splitter causes splitting of one beam into beams. One of the beams passing through sample arm travels towards the target sample and the other beam reaches the reference mirror passing through the reference arm. It is then reaching towards the beam splitter after reflecting back through the movable reference mirror Reflected light of the reference mirror then interacts with the light reflected from the target. Thus, interreference fringes are produced. After this, these signals are then interpreted and electronically processed to identify reflectivity values of the target as a function of the depth into the tissue. The scanning depth can be sweep by changing the path length of the reference mirror. Near infrared light (NIR) are usually used for OCT because the light is spatially enough coherent enough to be focused as well as incoherent temporally enough to carry multiple wavelengths. A schematic diagram of OCT system is shown in figure 1.5.

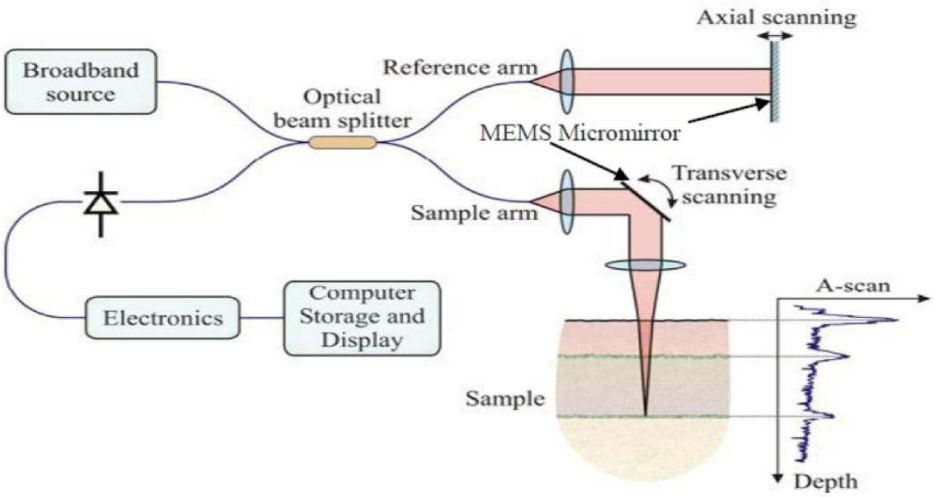

Figure 1.5: Schematic of the OCT system with integrated 2D MEMS micromirror [37].

Unlike a basic camera image that gives only planer information, it also scans depth of a target object. The OCT depth resolution is enough fine, typically on the order of 0.01mm. Now, the ultimate goal in this area is to minimize the size of OCT system with maximum deflection angle for endoscopic imaging. In MEMS micromirrors, the research has been focused on developing the micromirrors that can act as suitable reference mirrors and rotating mirrors to rotate light beams to scan target tissue areas.

The optimization of the device is carried out using design of experiment-based techniques. Optimization in our design is referred to design an optimal device, the configuration of which is based on a set of desired response and constraints. This has been achieved traditionally by developing mathematical models, genetic algorithm, artificial neural networks and FEM modelling. These techniques serve well, but in case of complex designs as in proposed micromirror, these methods have many limitations like too much computational cost is required and many assumptions are taken while modelling which lead to incorrect modelling of some complex designs. So, a design of experiment-based technique is used to optimize the deflection angle, input power and temperature rise of our micromirror device along with reducing the cost.

Chapter 2: Design of Actuators and Micromirror

Designing micro micromirrors, using MEMS fabrication technique rules, is different from designing large-scale machines. Among various MEMS fabrication techniques, polymer-based fabrication technique is selected for designing this micromirror. The polymer commonly used is SU-8. SU-8 is an epoxy based negative photoresist, which has been used for fabricating MEMS device for past few decades.

The reasons for selecting the polymer technique are due to its low cost, biomedical compatibility and low power consumption. Polymer is cheaper than metals and silicon, and easy to use. Biomedical applications require manipulation process at room temperature with no electrical conductivity due to electrolysis. It is compatible with biomedical applications, as it is a non-conductor of electricity and has a very low coefficient of thermal conductivity. Since SU-8 polymer is a non-conductor, thin layers of metals are deposited through electroplating to fabricate electrothermal actuator. Polymer based fabrication is a multi-layer process, so the heater of electrothermal actuator can placed at desired thickness between layers of SU-8. Overall thickness of SU-8 based design can increase by adding more layers of SU-8. To reduce the fabrication cost and complexity, this process requires only two masks for complete fabrication, one for SU-8 structure and one for gold heater and circuit.

2.1 Electrothermal Actuators

“Materials expand on heating and shrink on cooling” is the basic concept of Electrothermal Actuators. The change in temperature causes to expand the material. ETA is an actuator that uses this material expansion to actuate things.

2.2 Types of Electrothermal Actuators

Electro thermal actuators are classified into two major types. They are mainly divided on the basis of differences in the structural layers of the actuator and the mechanism involved.

2.2.1 Single layer Electrothermal actuators

The first is the one which consist of only a single structural layer. When a voltage difference is applied at two arms the phenomenon of actuation is done on two ends of an actuator. Due to applied voltage at ends, a current is passed within the actuator, hence heating it due to joule heating.

Once actuator is heated up, then it expands in proportion to the value of Co-efficient of thermal expansion of the material. As a result, it gives an actuation according to the topology of the actuator. Some examples of these actuators are discussed below.

Ogando, K., et al. reported a fully compliant out-of-plane thermal actuator [38]. The out of plane displacement is achieved hinges hence allowing a full thermal expansion in actuator beam. The hinges at both fixed ends of the beam decide the out of plane displacement direction of the actuator whether its upside or downside. On the other hand, the hinges at sides of centre part are responsible of keeping centre platform balanced. The out of plane deflection in both sides is shown figure. He reported an out of plane deflection of 150nm at input power of 2mw.

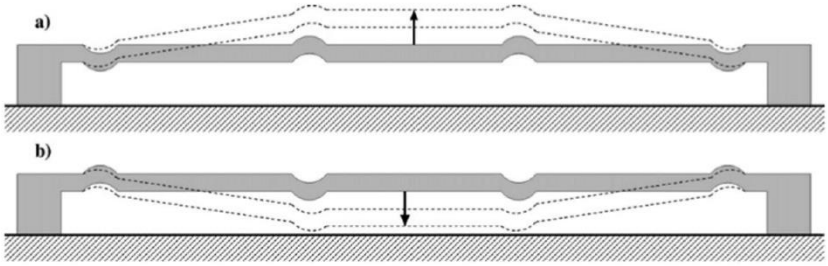

Figure 2.1: Electrothermal actuator proposed by Ogando, K., et al [38].

Kim reported a design of electrothermal actuator in [39, 40]. It also consists of a single structural layer beam, the beam has a step at both fixed ends, so once the voltage is applied, the beam is heated by joule heating and expands. So, the exerted by its expansion causes a couple of momentum and hence making an out of plane deflection in beam as it is shown in figure. Kim reported an out of plane deflection of 32um in [39] and 85um in [40].

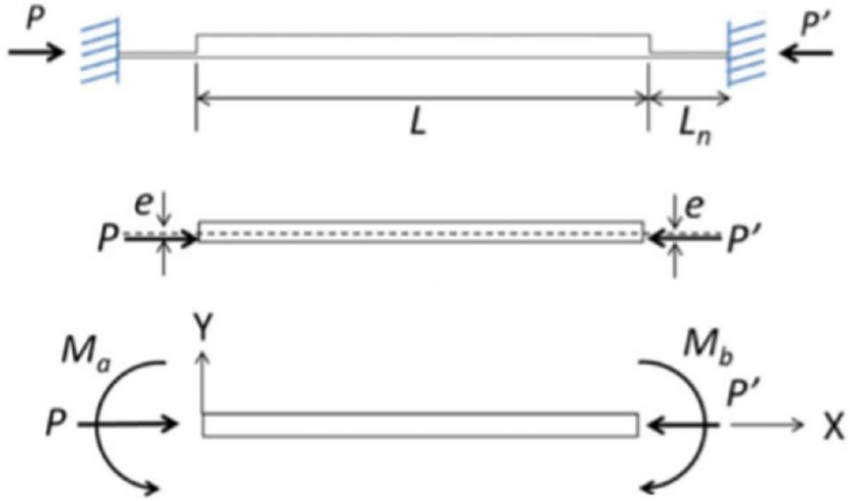

Figure 2.2: Electrothermal actuator proposed by Ogando, K., et al [38].

Venditte et.al reported an in plane bi-directional electrothermal actuator which consists of three legs beam just like W-shaped beam [41]. Centre leg has comparatively more width as compared to side legs as shown in figure. The actuator moves upward when a voltage is applied at A2 while AC and A1 kept at ground. And downward motion results from an applied voltage at A1 while other two ends are kept at ground. The working principle here is also depends on joule heating, when one of side legs are excited by an applied voltage, it heated up due to joule heating and hence expands more as compared to centre leg as its resistance is greater than centre leg. As a result of this expansion, an in-plane bending is occurred. Venditti reported a displacement range of 12um (6um in each direction).

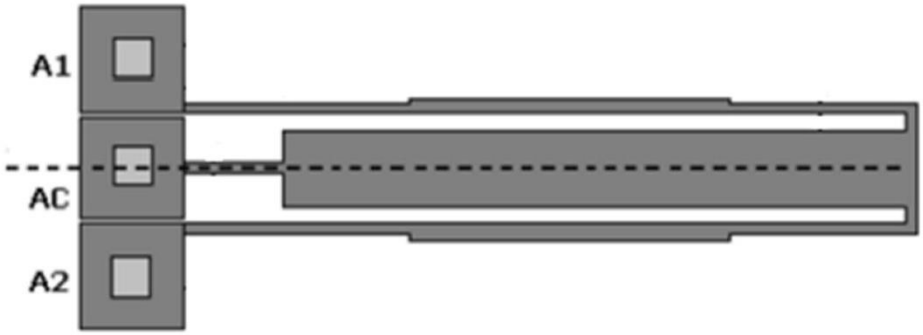

Figure 2.3 Schematic diagram of a bi-direction in plane Actuator [41].

We discussed above some of electro thermal actuators which contain only one material structural layer and cause a deflection in a result of thermal expansion by joule heating. The out of plane actuation can be observed as follows: -

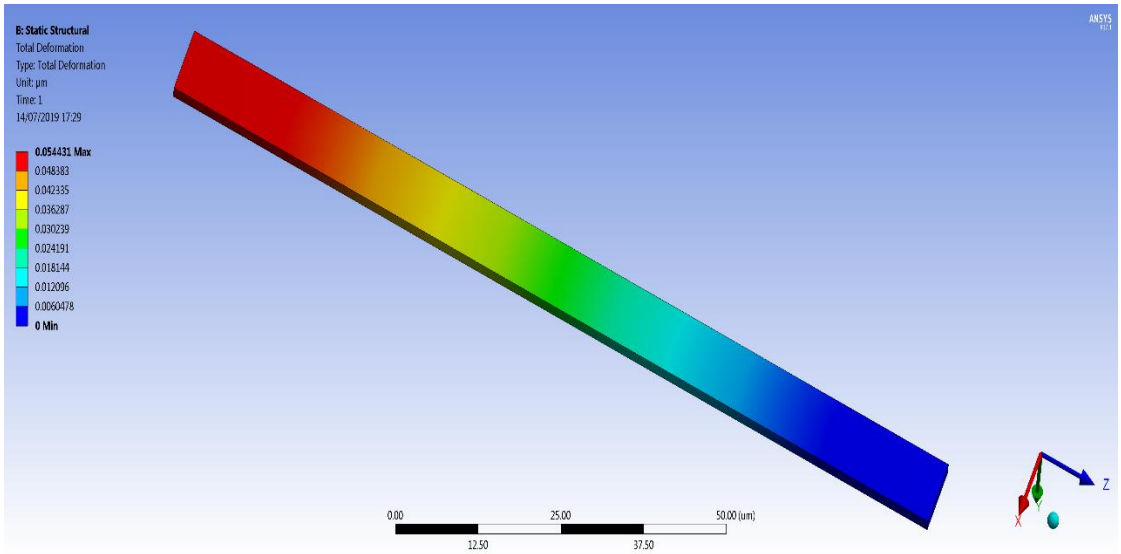

Figure 2.4 Out of plane displacement of Electrothermal Actuator.

The Single Material based Electrothermal actuators do have two kind of actuation deflections:

a) In-Plane deflection
b) Out of Plane deflection

Our choice of interest here is out of plane actuation to make our micromirror functioning well.

2.2.2 Bi-morph Electrothermal Actuators

The actuators consist of two structural layers are called bimorphs. The mechanism in these types of actuators involves conversion of thermal energy into transverse displacements. If we discuss bimorph actuator, it is cantilever beam contains two materials joined together sideways the length of actuator. Materials that are joined together are preferred to have high difference in the values of their coefficients of thermal expansion (CTEs). The higher the CTE means higher expansion when exposed to higher temperature and smaller CTE means less expansion at higher temperatures. So, the beam consists of two material layers which have a high difference in their CTEs, gives rise to a vertical out of plane displacement when applied to high temperatures because of different expansion rate.

Initially the temperature is normal at room temperature that is T_i, the beam is at its normal or stress-free state. When the temperature is changed due to joules heating, the change in length or in other dimensions' changes differently in both layers because of different values of CTEs. The difference in this change exerts a significant stress at the interface of both layers. The stress will be tensile in the layers with high expansion while compressive in the layer with low expansion.

2.3 Bending Stiffness

The bending stiffness of the curved beam device is an important factor to be considered. The curved beam bending stiffness is EI. Also, torsional rigidity of the curved beam is reported as GKt (uniform along the beam). The material considerations are linear elastic; also, E is the modulus of elasticity (Young's modulus) and G is the shear modulus. Deflection in a curved beam is expressed in the handbook of Roark's formula for stress and strain [18] suggests that as follow: -

$$\delta = \frac{\pi}{4}\frac{PR^3}{EI} + \left(\frac{3\pi}{4} - 2\right)\frac{PR^3}{GK_t} \tag{2.1}$$

Moreover, bending stiffness can be calculated as a ratio of force to deflection.

2.4 Stress Analysis

For any material layer, the deflection or strain can be expressed as:

$$\varepsilon = \alpha . \Delta T \tag{2.2}$$

Where ε in thermal strain in the material, ΔT is the change in temperature and α is CTE. According to Hook's

Law, the thermal stress (σ) is

$$\sigma = E. \alpha. \Delta T \tag{2.3}$$

Also, E is the selected Young's modulus of the material.

From above equation, we can see that the thermal stresses depend on Young's modulus, applied temperature difference and CTEs of the materials.

As beam bent out of plane from its undeformed state on deflection, so radius of curvature of beam at any time is given by [42]

$$\frac{1}{\varphi} = \frac{6\, w_1 w_2\, E_1 E_2 h_1 h_2 (h_1+h_2)\, \Delta\varepsilon}{(w_1 E_1 h_1^2)^2 + (w_2 E_2 h_2^2)^2 + 2 w_1 w_2 E_1 E_2 h_1 h_2 (2h_1^2 + 3h_1 h_2 + 2h_2^2)} \tag{2.4}$$

Where *E*,ε,*w*, and *h* are the Young's Modulus, strain, width, and the thickness of the beam layers respectively, while the subscripts 1 and 2 expresses the lower and upper layer of bi-morph actuator of micromirror. The strain is induced in each layer of the ETA due CTE due to thermal expansion principle. As the physical properties of both materials are different, so this strain will be different in both layers. This strain difference is induced only due to thermal stresses because we have neglected residual stresses so we can write as:

$$\Delta\varepsilon = \Delta\varepsilon th \tag{2.5}$$

From now onwards, we are going to discuss the methodology to design micro actuation and the selection of best material for bilayer micro actuator, which is the most important stage in any MEMS designing device. Critical reason of displacement and technique of actuation and are explained at first. Then the optimum materials to be used in these biomaterial actuators are discussed later.

2.5 Design of Optimum Structural Layer for ETA

It can be analysed from the relation that Young's modulus, Coefficient of Thermal Expansion (CTE) and temperature difference applied of the single structural layer are the affecting properties the stress. The actuator with thermal bimorph covers two materials which are along the length attached. The actuator will give deflection on heating or cooling because of difference in coefficients of thermal expansion of materials. As both the materials are "glued" together, so the in-plane extension changes displacement out of plane. Materials with high CTE difference should be used to maximize the displacement.

In MEMS, the most important aspect to be considered while designing is materials selection as it determines thermo-physical phenomenon such as cost economics, thermal time constant for dynamic analysis, maximum displacement for static analysis, compatibility with micromachining and maximum temperature change. Some of the electrical properties are also directly or indirectly related to the thermal properties of material, like resistivity, heat dissipation, thermal conductivity, etc. This also affects the power usage, and the requirement while designing electronics, is always low power usage. There is always a trade-off between the thermal conductivity and CTE in selection of material because the maximum deflection is directly proportional to the difference of CTE. High frequency. That’s why we have chosen Gold along with the SU-8 material for its being suitable material pair with SU-8.

Since the polymer does not conduct electric current, additional layer of metal heater is added to the actuator design. The heater in actuator is made of gold. For the required Out of Plane motion the Gold base with a single layer of SU-8 is used.

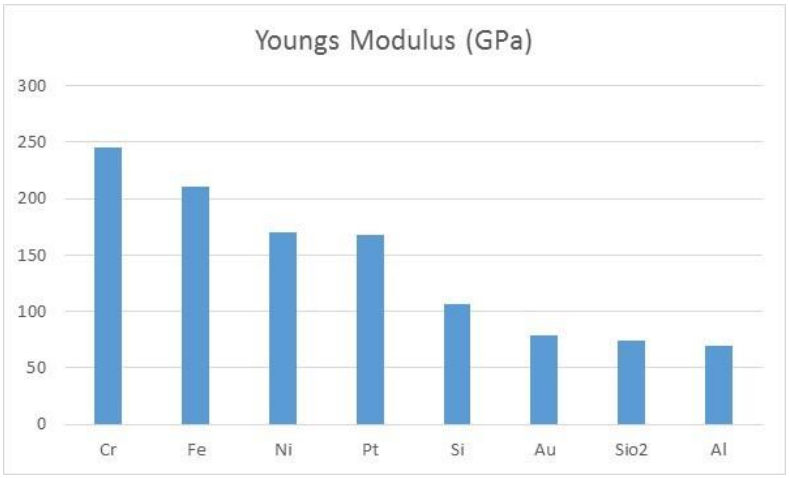

Figure 2.5: Young's Modulus Comparison of materials commonly used in MEMS.

Table 3: Material Properties Comparison

Material Properties	SU-8	Gold
Young's Modulus	4.60	70
Poison Ratio	0.22	0.35
Density	1200	19320
Specific Heat	1674.8	128
Coefficient of Thermal Conductivity	0.2	300
Coefficient of Thermal Expansion	52×10-6	14.2×10-6
Electrical Resistivity	-	2.4e-8

2.6 Design and Modelling of Electrothermal Actuator

In this section, the design and operation principle of electrothermal bi-morph actuator is discussed in terms of design.

2.6.1 Design of Curved concentric Geometry

A curved concentric electrothermal actuators based micromirror design has been developed to acute these circular micromirrors with improved device size. It gives displacement at scan angles with low actuating voltages. The small side deformation shifts and tilt of these mirrors are best for applications where the four actuators one-time movement is required. The side shift and tilt can be additional minimized by reducing process variations, using more fast design, and tuning the drive signals fine. Also, concentric curved actuators and the curved circular micromirror device results incompact device size. In the past only few such designs were made for in-plane movements. There was no such design which can show out of plane actuation.

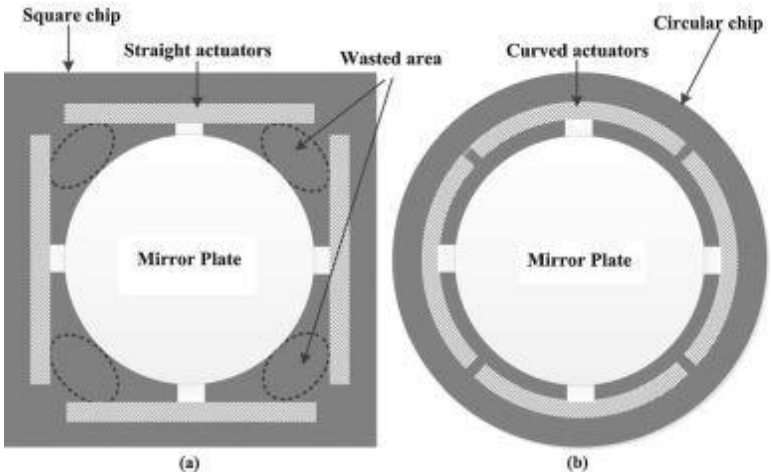

Figure 2.6 (a) Circular mirror with straight actuators. (b) Circular mirror with curved actuators. [43].

2.7 Design of an Electrothermal Actuator

In this section a complete summary of the proposed ETA is given. The materials pair are selected as Gold and SU-8 as with least dimensions taken. It consists of three arms i-e External Arm, Internal Arm and Thin Arm. They are all joined by a connector together. There are also flexures attached at the two wide arms the dimensions of the actuator are taken as lengths to be 256um,158um,196um, widths to be 8um,3um and 8um and thickness to be 6. A diagram of electrothermal actuator is shown in figure 2.7.

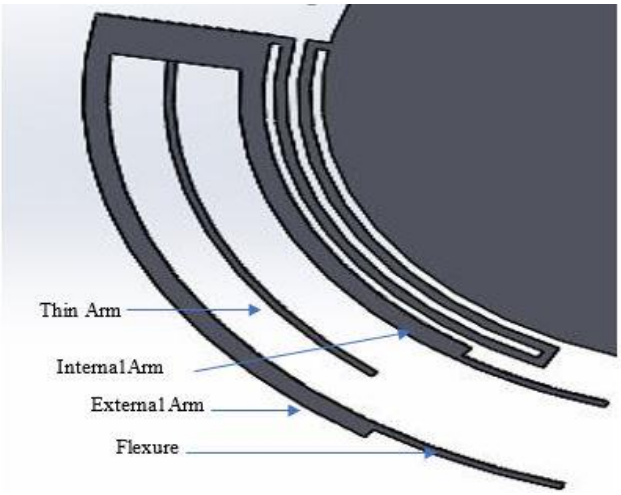

Figure 2.7 Design of Electrothermal actuator.

2.8 Design of Micromirror

In the application of OCT, mirror curvature has an important effect on imaging because mirror surface affects the incident light beam and hence affecting the coupling efficiency and

resolution of the imaging [44, 45]. We have designed our mirror keeping all these factors in mind so that tendency of stress resulting in curvature is reduced. The reflectivity of different metals used in MEMS is reported by [46]. It can be seen that gold has a good reflectivity of $R = 0.89129$ at 0.5876 µm. So, our mirror consists of gold device layer as a structural layer with gold also reasonable it for reflection. 5um.However, temperature of heater must not reach above 200°C, as SU-8 has low melting point. The voltage levels must be below 1.29 V to avoid the process of electrolysis, which is not a problem due to thin heater design We used a mirror with 2µm gold with a mirror size of 300 µm x 300 µm.

One of the limiting factors in the design of high frequency micromirrors is dynamic deformation that are intended for high definition fast scanning display applications. High acceleration loads cause beam divergence, which will in turn reduce the optical resolution. There are different types of plates with respect to shapes: -

a) Diamond Shaped Mirror plate
b) Circular Shaped Mirror Plate
c) Rectangular Shaped Mirror Plate
d) Octagonal Shaped Mirror Plate
e) Pentagonal Shaped Mirror Plate

As it is observed that Circular Shaped Micromirror showed better agreement to the design as dynamic deformation was reduced in it.

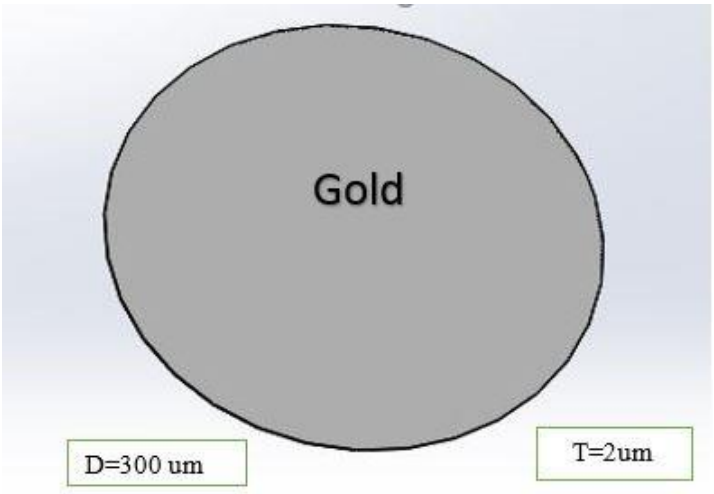

Figure 2.8 A schematic diagram of micromirror.

2.9 Design of Flexural Springs

The mirror plate of 300x300 µm area is attached to four electrothermal actuators through flexural springs. We have made U shaped springs in curved form which make the geometry more concentric. The schematic details of U-shaped spring is expressed in figure 2.9

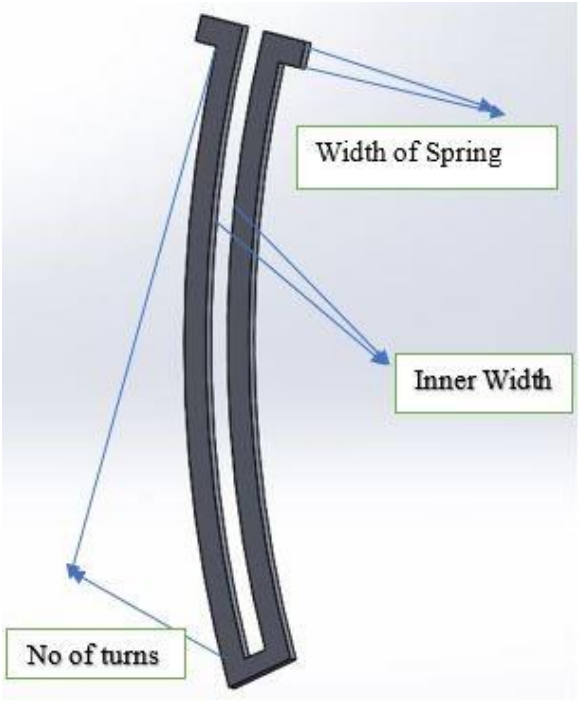

Figure 2.9 Schematic of U-shaped spring.

R. Liu [49] analysed the concentration stress and stiffness changes by the basic parameter of all types of springs which is: -

1) If we increase the thickness of the flexure springs, stiffness increases and stress decreases by doing the same increment in thickness of flexure springs.
2) A decrease in the stress and stiffness is noticed when we increase the straight length of the flexure spring.
3) Stress and Stiffness both increase with increment in the width of the flexure spring.
4) Stress and stiffness both decrease if we increment the inner diameter of the flexure spring.
5) Stress and stiffness and both decrease if we increment the number of turns of the flexure spring.

The number of turns of the flexural springs is of vital importance as it affects the stiffness and stress. In our design, the flexural springs are made of silicon device layer of SOI wafer. A

design of complete micromirror device is shown in figure 2.10. Optimization of the device dimensions and layout is discussed in next chapter.

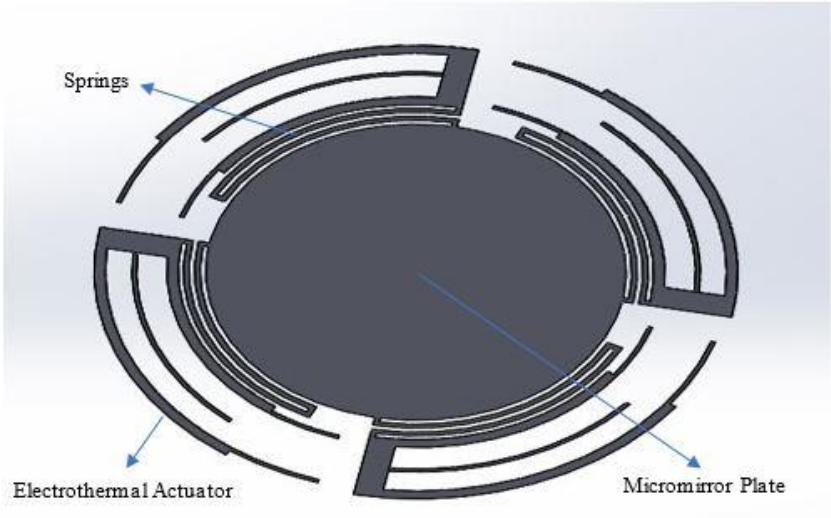

Figure 2.10 Design of micromirror with flexural springs.

Chapter 3: Finite Element Method Based Modelling

The finite part technique could be a computative technique to manage issues of engineering and mathematical physics. Typical downside areas of interest embrace structural analysis, fluid flow, heat transfer, mass transport, and magnetic attraction potential.FEM based Electro-Thermal and Thermo-Mechanical Analysis.

3.1 FEM based Electro-Thermal and Thermo-Mechanical Analysis

In this Chapter, a comprehensive FEM primarily based simulation methodology is undertaken for the planned small mirror. The FEM could be a numerical technique for getting approximate answer of the partial differential equations. The small electrothermal mechanism is ruled by these partial differential equations that in result divides the small mechanism domain into a mesh of separate sub domains known as the finite parts. Then approximate polynomial solutions of those partial differential equations square measure found by these finite parts. Then, to offer a complete answer with AN applicable degree of smoothness over the whole small mechanism domain, the approximate polynomial results of every part square measure pieced along. though absolutely the results of the FEM simulation is subject to approximation errors, sure accuracy will still be achieved with applicable meshing structure.

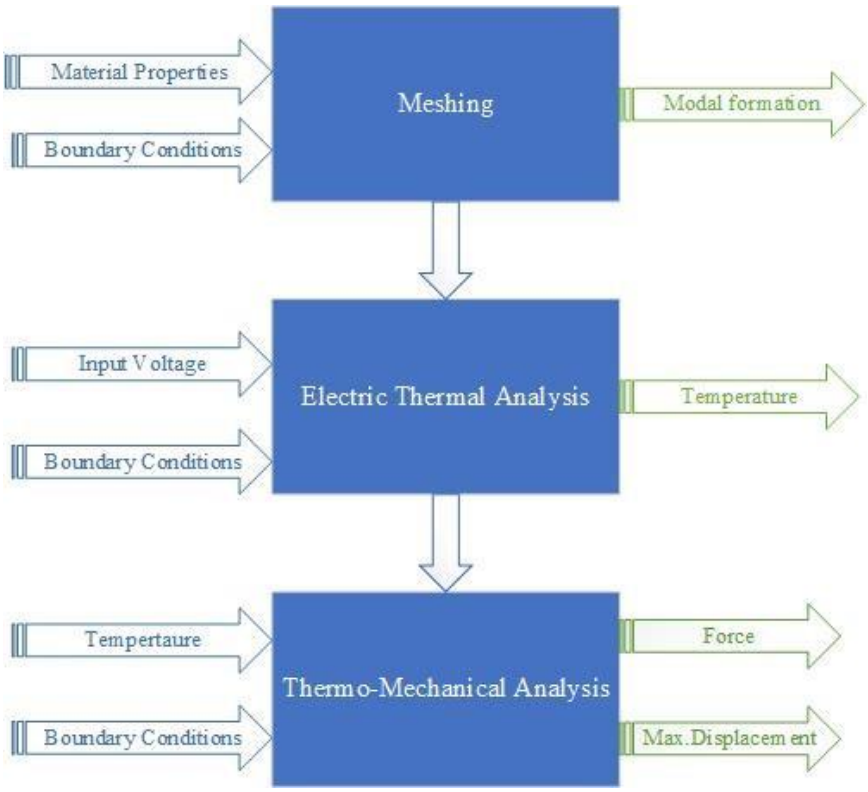

Figure 3.1: The sequential diagram for performing the FEM-based simulations.

The input parameters of the design analysis are shown by the blue arrows in sequential diagram for performing FEM based simulations whereas the outcomes are shown by the green. To perform these two analyses, we used Ansys 17.1 workbench, whereas the geometries were made on the Solid woks 2017. For the analysis we selected the analysis systems as follow: -

a) Thermal Electric
b) State Structural Analysis

3.1.1 Electro-Thermal and Thermo-Mechanical Analysis for Actuator

For the electrothermal actuator, an Electrothermal analysis is initially executed to estimate the per degree temperature rise from ambient on the beams of the ETA & on the micromirror plate for an applied actuation voltage. By increasing actuation voltage there is noticeable increase in the temperature of electrothermal actuator beams. But the maximum temperature on the hot arms of the electrothermal actuator& micromirror plate is less 20 $°C$ even for the applied voltage of up to 0.04V. Temperature profile of the proposed MEMS micromirror in Figure 3.2 presents that the

maximum temperature is present on the electrothermal actuator beams while there is negligible temperature rise on the proposed micromirror.

Temperature values found through the electro-thermal analysis are used in FEM based thermo-mechanical analysis to determine the maximum output displacement along with the output force generation through chevron shaped electrothermal actuator. For an applied input actuation voltage of up to *0.04V* the corresponding values of maximum out of plane displacement produced by the actuator are shown in Figure 3.4. The thermo-structural analysis results depict the increasing trend of both the output displacement increasing the input actuation voltage. Maximum displacements produced by the electrothermal actuator are micrometers.

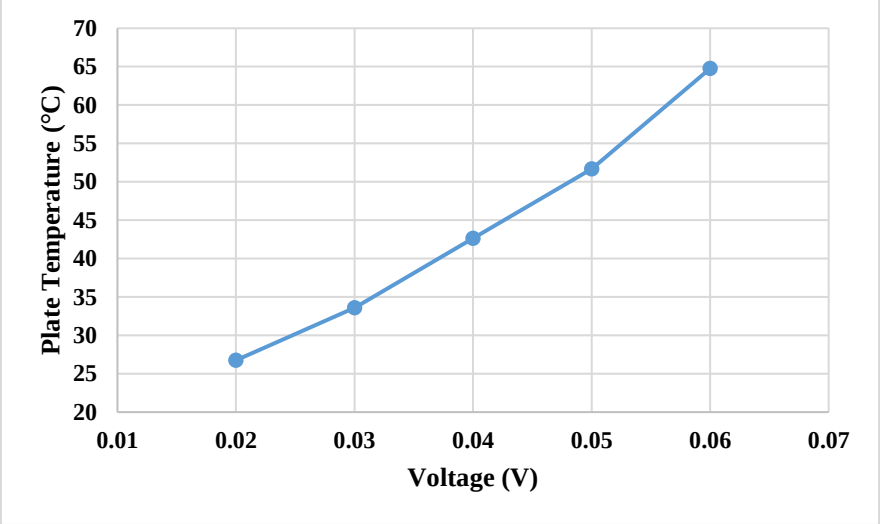

Figure 3.2: Temperature rise corresponding to the applied input voltage.

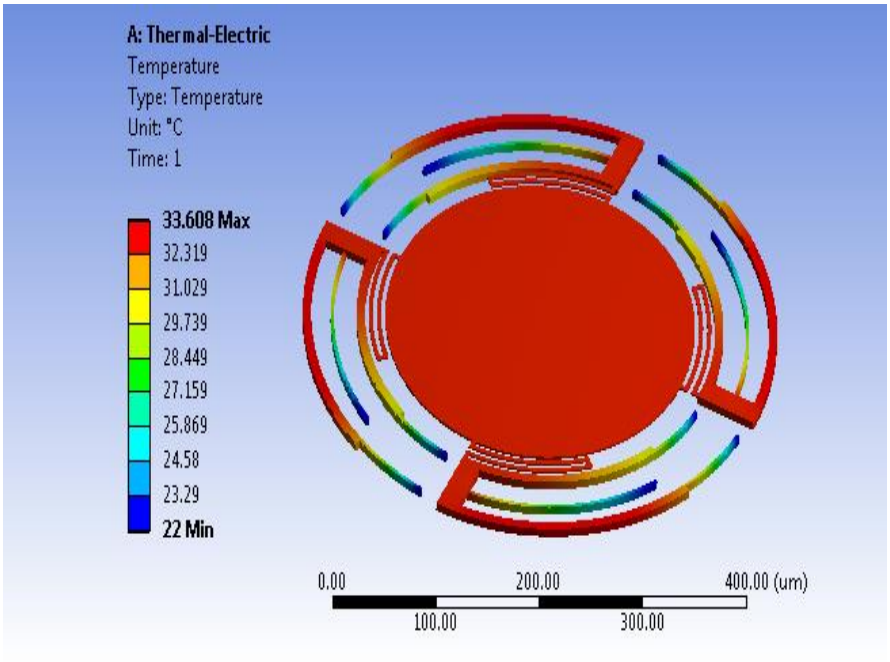

Figure 3.3: Temperature profile of the proposed micromirror design

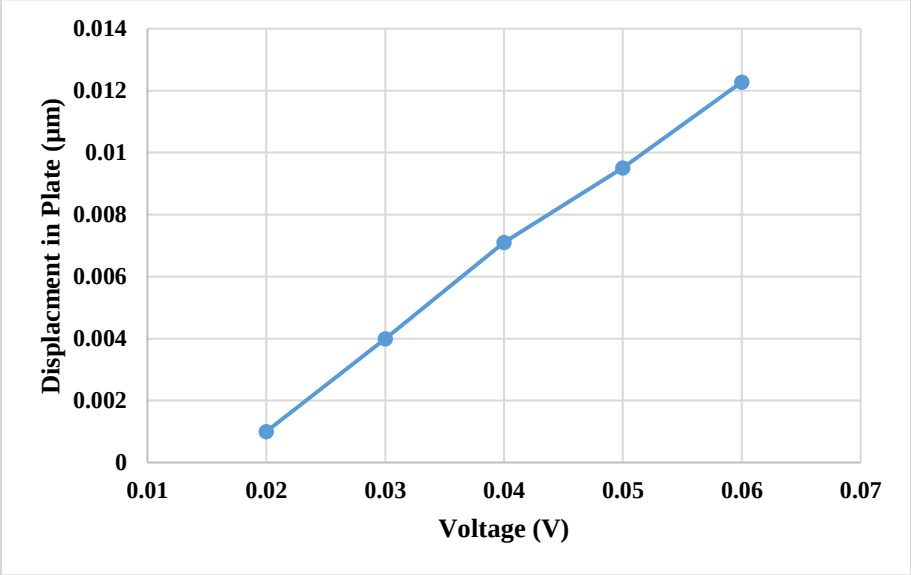

Figure 3.4: Maximum displacement generation corresponding to increasing values of the input actuation voltage.

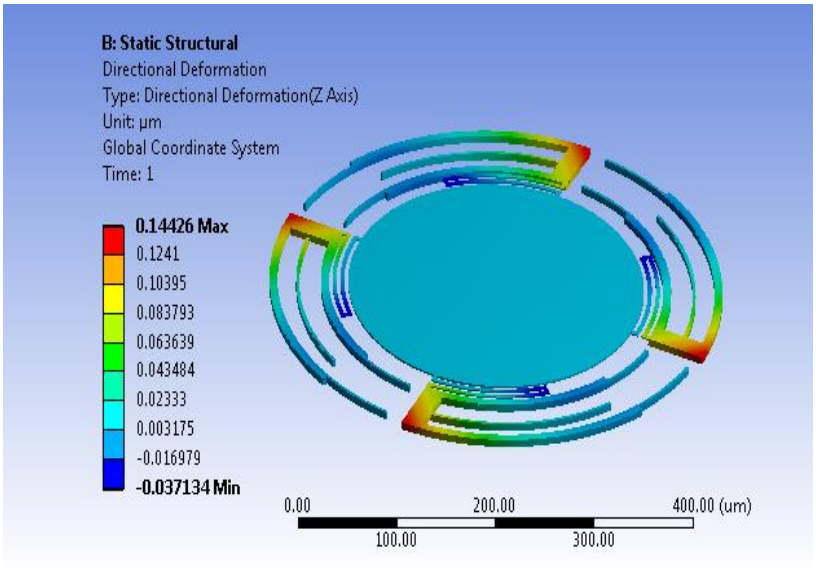

Figure 3.5: Thermo-mechanical analysis presenting the maximum output displacement attained by the proposed micromirror corresponding the applied voltage of $0.04\ V$ dc.

As declared before, the arms of the thermal mechanism are separated from the substrate by an air gap. some of the warmth generated is lost through the air. The mode of this heat transfer depends on the pure mathematics and setup of the actual device. It's been ascertained that as devices are scaled all the way down to the microlevel, conductivity dominates the warmth transfer. The temperature of the outlet body of ETA and encompassing is at temperature. ab initio the pads of the mechanism were mounted and a step electric potential (DC) is applied as precondition.

The complete thermo-elastic drawback considers the temperature and strain to be mutualist. The temperature field causes thermal enlargement, that contributes to the strain field. The modulus and also the constant of thermal enlargement are enthusiastic about temperature. Heat generated thanks to the work of deformation is negligible thereto generated by Joule heating. The elastic drawback so depends on temperature however not the other way around. Since the encompassing air and substrate don't have an effect on the mechanism deformation, they were eliminated from the model to extend machine potency. A nonlinear resolution was needed thanks to dependence of thermal enlargement constant on temperature and enormous thermal deformations of the mechanism arm Stiffness of the Flexures

As mentioned earlier, we have used U shaped curved spring to attach the micromirror plate with the ET actuators to check the extent to which the design resists the deformation against

applied voltage. It is the moment required to produce unit rotation in the device. It depends upon the Elastic Modulus, Moment of Inertia and Length of the member. It is basically a ratio between force creating the deformation where *Ls* is the length of spring, *E* is the modulus of Elasticity, *t* and *w* are thickness and widths given by Eq. (3.1) respectively.

$$K = \frac{Etw^3}{L_s^3} \tag{3.1}$$

For curved geometry we can calculate the stiffness by the deflection the quarter-circular beam with the free end of can be found in for stress and strain with Eq. (2.1).

Moreover, the stiffness of the springs can be found out with help of Ansys Static Structural analysis. If we apply a certain amount of force and we see the deformation against this value we can calculate any kind of shape possessing springs. The FEM results for deformation against 10 um of force results in 416 N/m stiffness as shown figure 3.6.

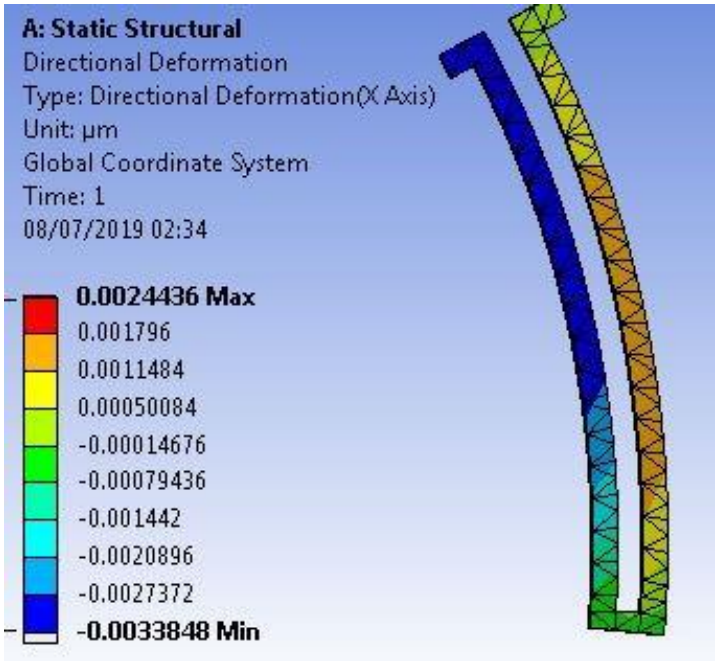

Figure 3.6: Deformation analysis of the Curved U-shaped Flexure.

3.2 Comparison between Rectangular and Curved Geometry

In past years, we have seen that there were few designs that were made from single material for Out of plane deflection of micromirrors. All of them were almost made in Rectangular geometry having a high device size also. In our design, we have made a curved concentric shape to reduce the size and increase the efficiency. We have implemented the same design in curved and rectangular form with same dimensions to compare the results provided the same boundary conditions.

3.2.1 Input Power

Provided the same boundary conditions, with $0.03V$ as the operating voltages applied on all the four actuators in piston mode leads to the higher input power of 1.07 mV in Rectangular geometry and 0.056 mW as in our design.

Input Power=Current density*Area of cross-section*Applied Voltage

3.2.2 Device Size

The device size of the rectangular geometry is 600µm*600µm but with same dimensions we achieved a device size of 460µm*460µm.

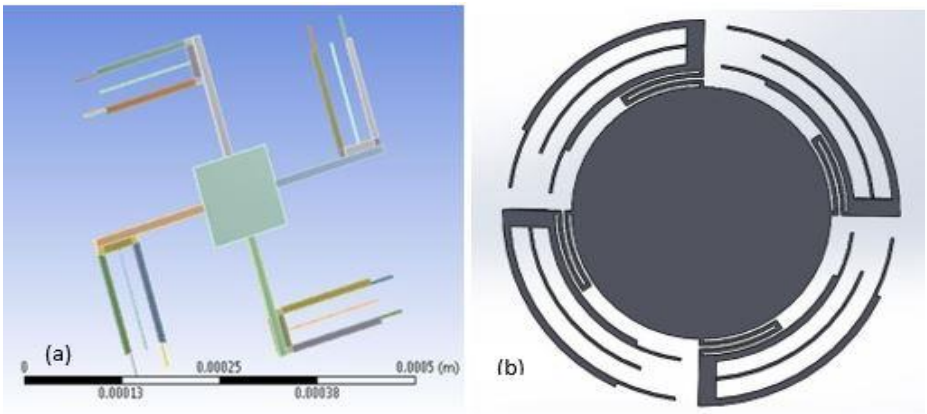

Figure 3.7: Comparison between Curved and Rectangular geometry. (a) Rectangular. (b) Curved.

3.2.3 Temperature Rise

In our problem statement we needed a design to have the minimal temperature rise from the ambience on the mirror plate, to increase its life. As the voltages applied and room temperature conditions were applied, we got the temperature rise which was imported as a load to the Thermo mechanical analysis. As both the designs were compared the temperature rise for Rectangular geometry was seen to be 26 degrees more than room temperature and for that of Curved geometry it was seen to be 11 degrees only.

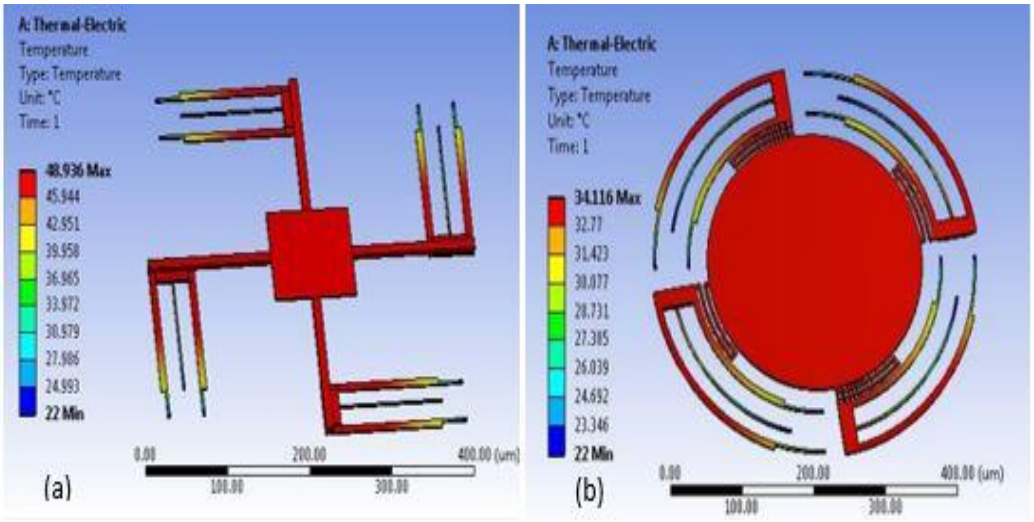

Figure 3.8: Comparison between Curved and Rectangular geometry. (a) Rectangular. (b) Curved.

3.2.4 Displacement

Once the imported load of temperature is provided to the Thermo-Mechanical system, the deformation leads to Out of plane displacement for the design. Out of displacement of 0.03um was seen for curved geometry which was far better than 0.003um in Rectangular geometry.

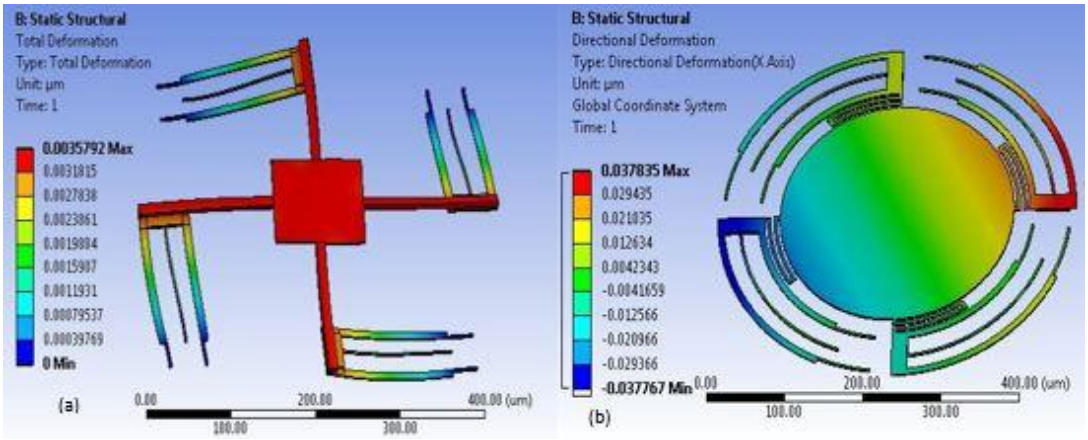

Figure 3.9: Comparisons in out of plane displacement. (a) Rectangular. (b) Curved.

3.2.5 Comparison

After all the observations and simulation results of both the geometries, it was clearly observed that all the parameters of the reasoning clearly justify Curved Geometry to be far better than the Rectangular one. It gives the highly optimized results which well defines the problem solution. The desired outcomes of out of plane deflection, device size, input power of the device and temperature rise from ambient well satisfied with the Curved Geometry.

Chapter 4: Parametric Analysis of Proposed Micromirror Design

In this Chapter, a comprehensive study of the design parameters is done with help of the Parametric approach. The design was studied for the desired three outcomes with all possible design parameters out of which the significant design parameters were deeply studied which effected the overall device results. Their behavior resulted in the best optimized geometry for this device.

4.1 Desired Objective Device

The results obtained from simulations analysis of basic design are additional investigated by execution of an optimization with our three goals simultaneously. We have set a design of Design factors which effect the overall design. Our goal is to check the effect of all the eight design factors to get an optimized solution with best results. We can observe from the parametric analysis that variables which are significant for all three output responses. So, we analysed the effect of these variables on all three output responses at an optimum level of all other design variables.

Table 4: Design Parameters

Factors	**Full names**	**Units**
LEA	Length of external arm	μm
LIA	Length of internal arm	μm
WTA	Width of thin arm	μm
LTA	Length of thin arm	μm
LES	Length of external spring	μm
LIS	Length of internal spring	μm
LEF	Length of external flexure	μm
LIF	Length of internal flexure	μm

Table 5: Output Responses

Responses	Full names	Units
IP	Input Power	mW
DP	Displacement in Plate	μm
PT	Plate Temperature	$℃$

Our mirror design is optimized on the basis of the objective function given below: -

a) Displacement should be maximum
b) Input power should be minimum
c) Temperature rise < 30K

The Micromirror design parameters can be observed clearly by the following figure 4.1.

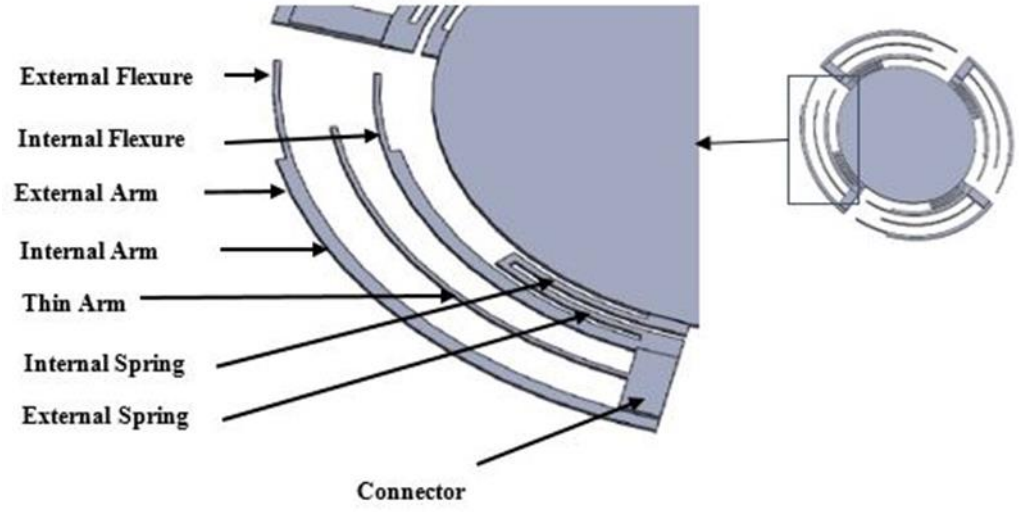

Figure 4.1 A complete Schematic of all design parameters

4.2 Effect of Geometric Parameters on Micromirror Responses

The whole geometry was observed to made up of its constituents' parameters to have some effect on the responses. We one by one fixed all of our parameters and vary only one parameter to check its behaviour and create design curves. It helps to observe the behaviour of the performance parameters. Our main goal is to design the optimized geometry to meet the best possible outcomes of it.

4.2.1 Effect of External Arm

Parametric Analysis generated the design curved varying the length of the Curved shape External arms to check its effect on the three outcomes. It is observed from the data range of the Output responses with figures 4.2 (a), (b) and (c) that the best results could be gained when the Length of external arm reaches at the value of 256 µm. In order to make the geometry optimized the trends show LEA to have maximum value.

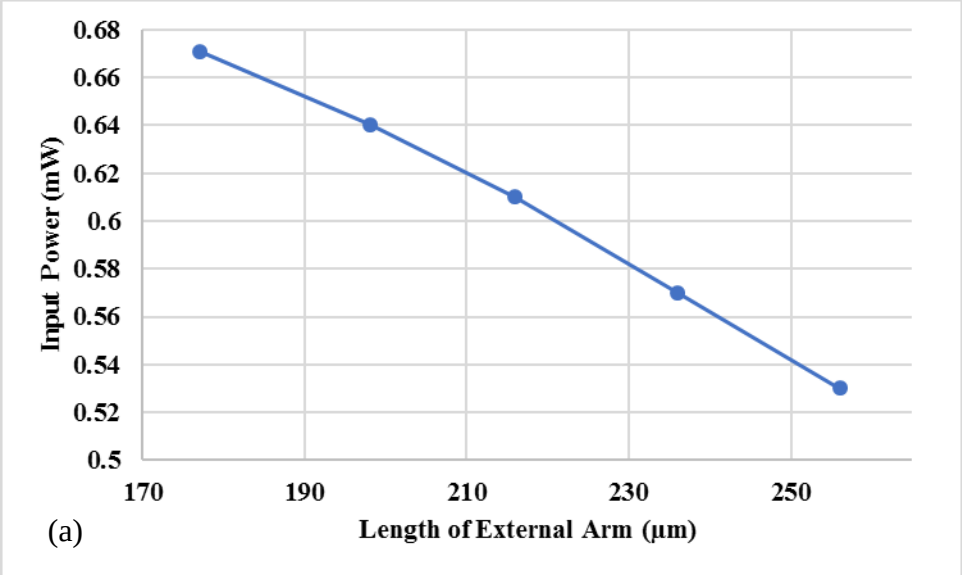

(a)

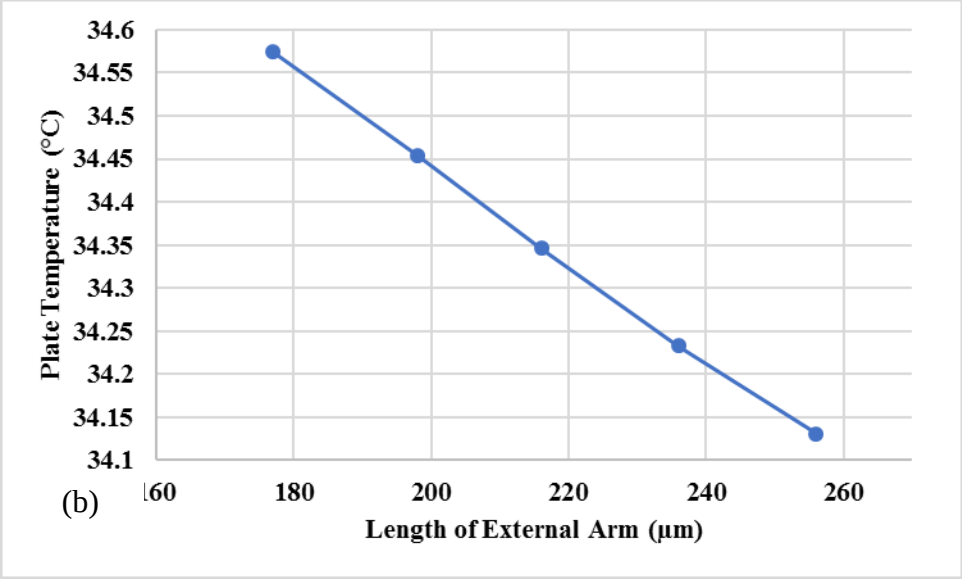

(b)

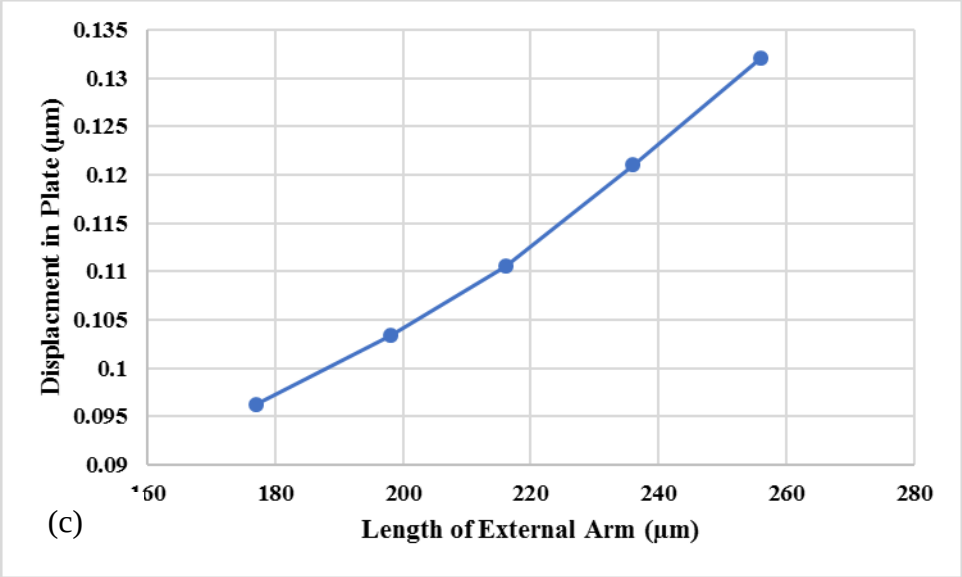

(c)

Figure 4.2: (a) LEA varying with PT. (b) LEA varying with IP. (c) LEA varying with DP.

4.2.2 Effect of Internal Arm

The design curved varying the length of the Curved shape Internal arms to check its effect on the three outcomes were observed. It is observed that at the value of 196 µm from the data range of the Output responses the best results were gained. In order to make the geometry optimized the trends show LIA to have maximum value as observed from figure 4.3(a), (b) and (c).

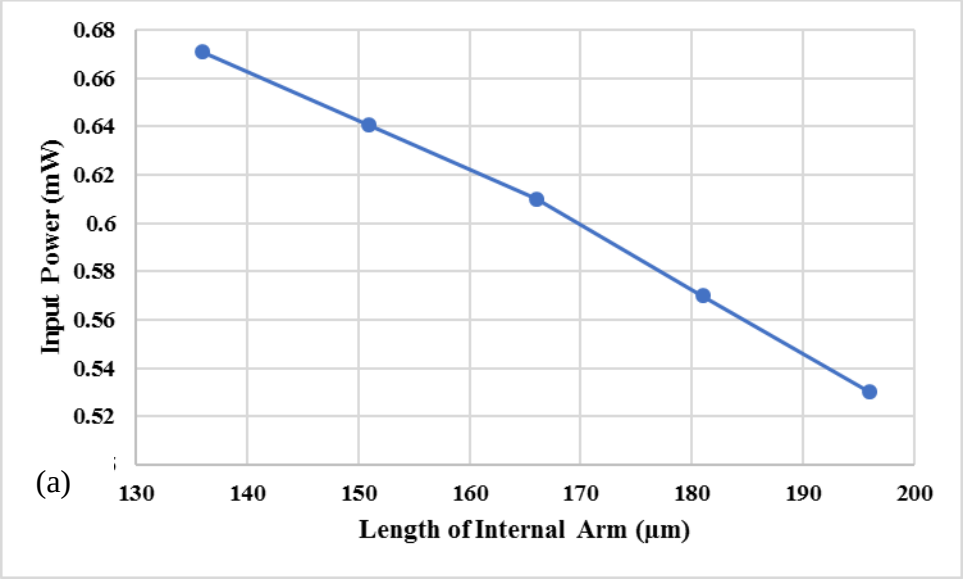
Input Power (mW)
0.68
0.66
0.64
0.62
0.6
0.58
0.56
0.54
0.52
130
140
150
160
170
180
190
200
Length of Internal Arm (µm)

(a)

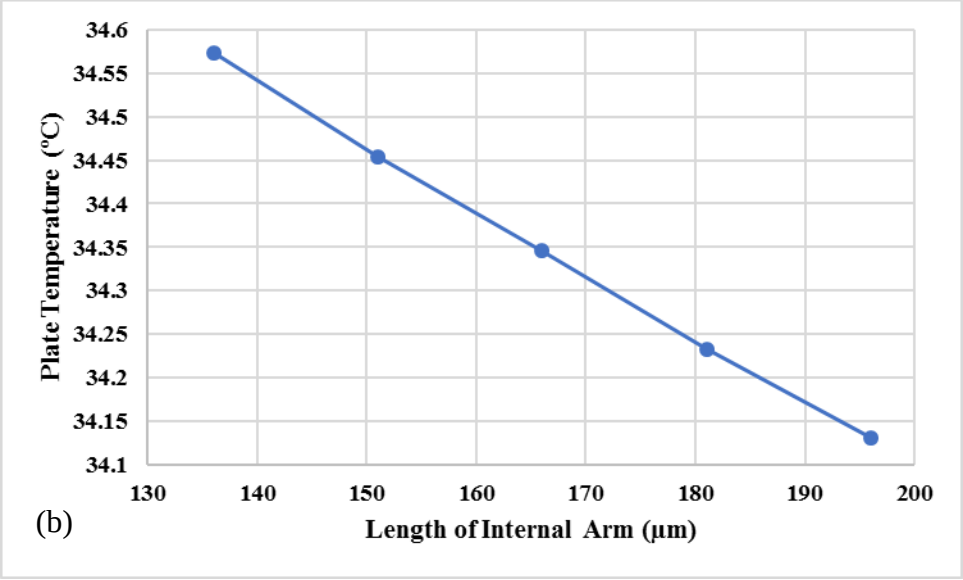
Plate Temperature (°C)
34.6
34.55
34.5
34.45
34.4
34.35
34.3
34.25
34.2
34.15
34.1
130
140
150
160
170
180
190
200
Length of Internal Arm (µm)

(b)

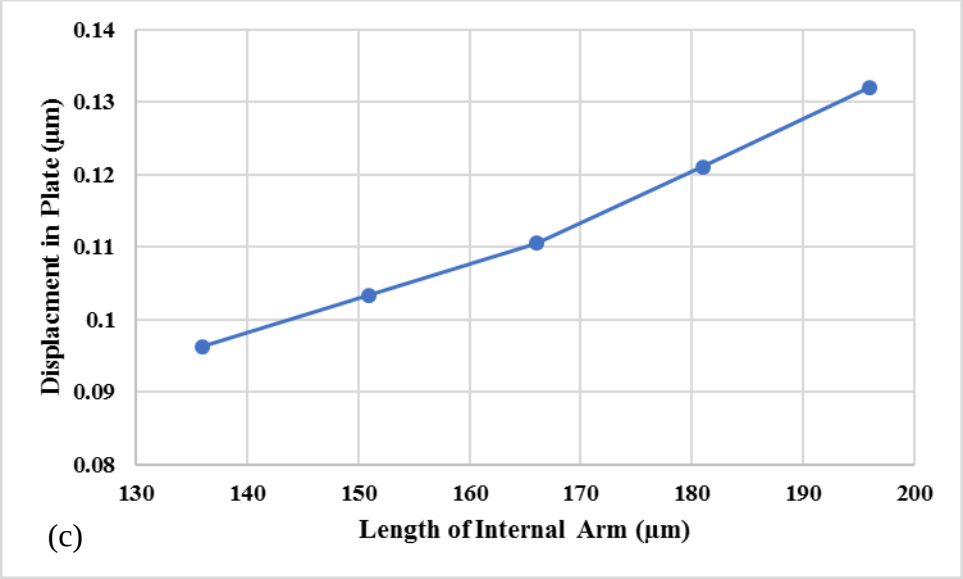

Figure 4.3: (a) LIA varying with PT. (b) LIA varying with IP. (c) LIA varying with DP

4.2.3 Effect of Thin Arm

The thin middle arm varying behaviour trend was observed with the desirable outcomes. It is observed that at the value of 246 µm from the data range of the Output responses the best results were gained. As observed from figure 4.4(a), (b) and (c), in order to make the geometry optimized the trends show LTA to have maximum value.

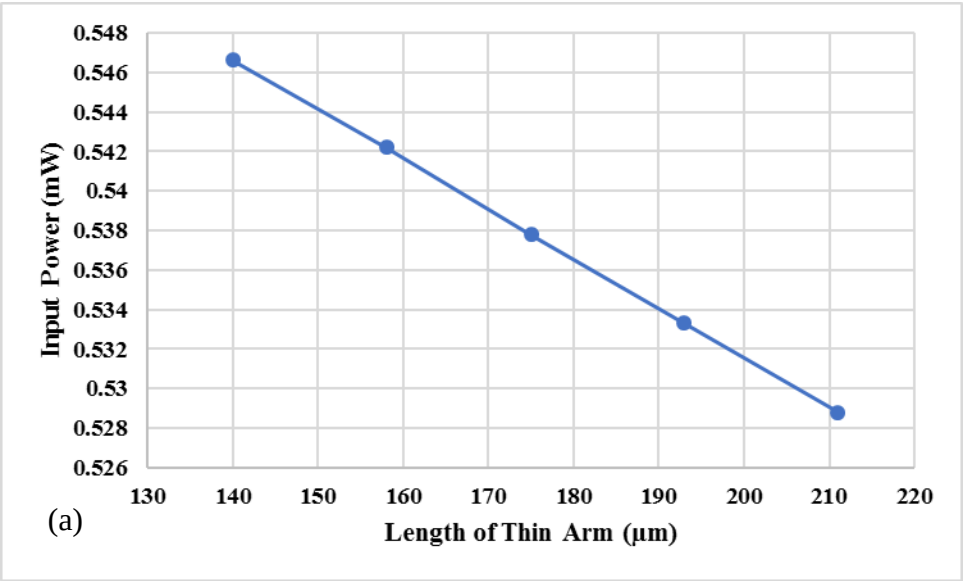

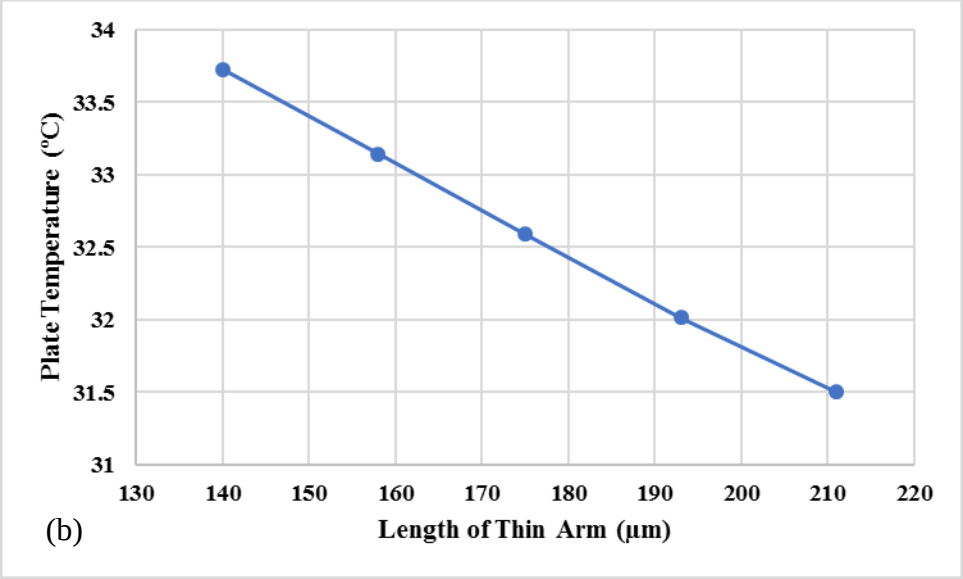

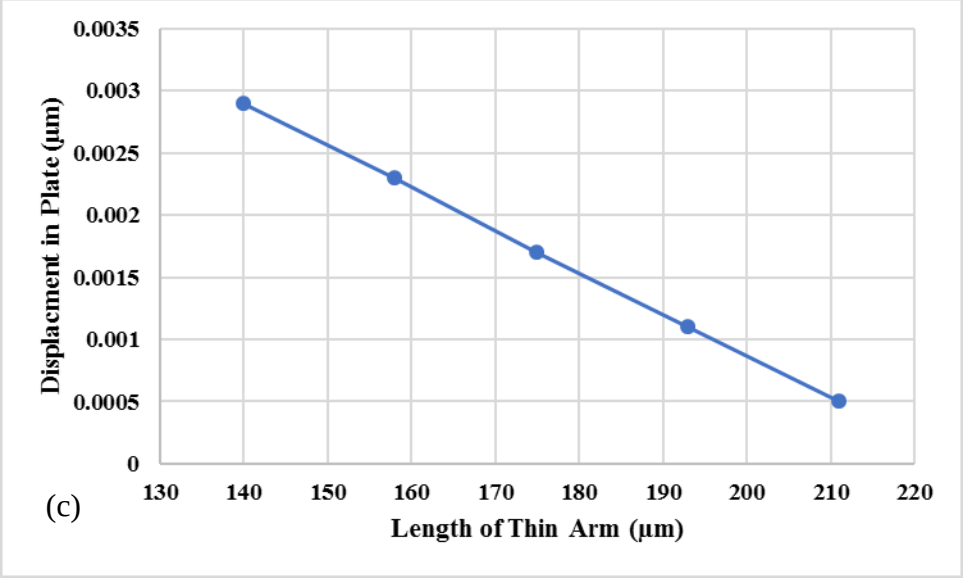

Figure 4.4: (a) LTA varying with PT. (b) LTA varying with IP. (c) LTA varying with DP.

4.2.4 Effect of Length of External Spring

The Length of External Spring varying behaviour trend was observed with the desirable outcomes. As observed from figure 4.5(a), (b) and (c), in order to make the geometry optimized the trends show LES to have maximum value.

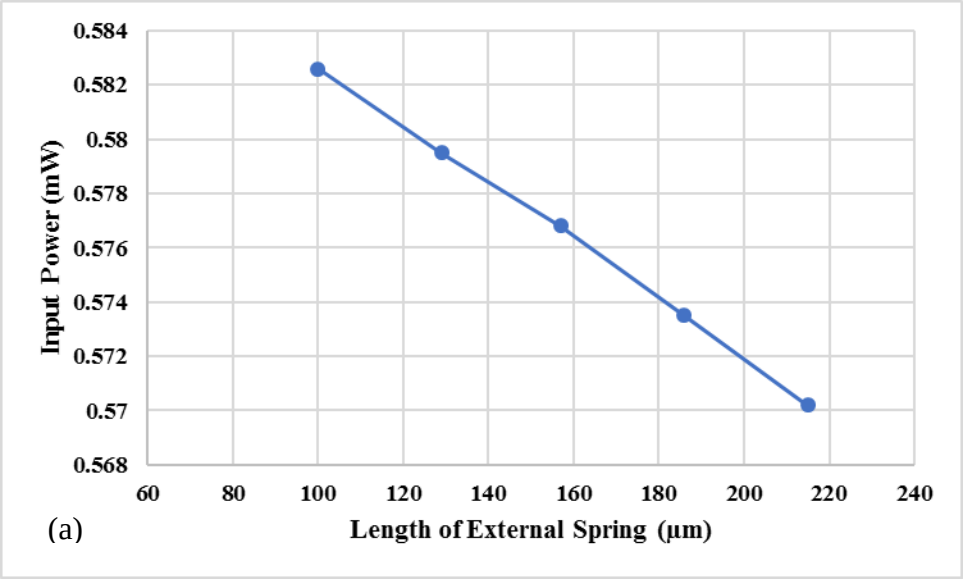
0.584
0.582
0.58
0.578
0.576
0.574
0.572
0.57
0.568
Input Power (mW)
60
80
100
120
140
160
180
200
220
240
Length of External Spring (µm)

(a)

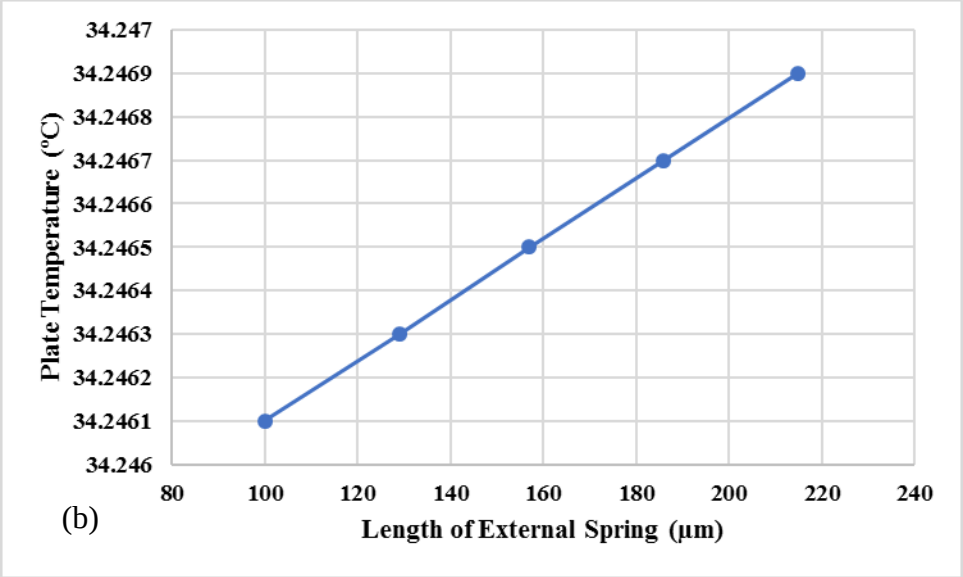
34.247
34.2469
34.2468
34.2467
34.2466
34.2465
34.2464
34.2463
34.2462
34.2461
34.246
Plate Temperature (°C)
80
100
120
140
160
180
200
220
240
Length of External Spring (µm)

(b)

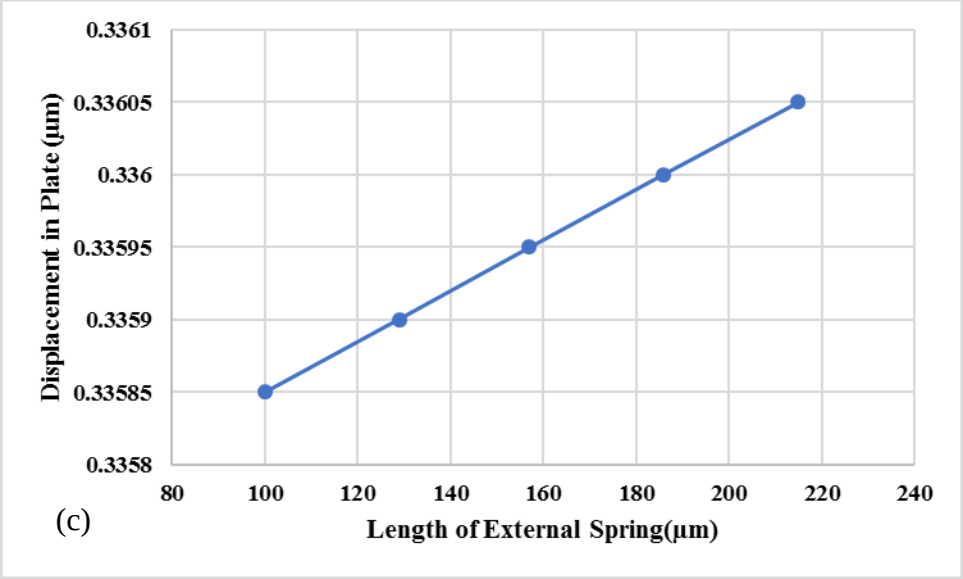

Figure 4.5: (a) LES varying with PT. (b) LES varying with IP. (c) LES varying with DP.

4.2.5 Effect of Length of Internal Spring

The Length of External Spring varying behaviour trend was observed with the desirable outcomes. As observed from figure 4.6 (a), (b) and (c), in order to make the geometry optimized the trends show LIS to have maximum value.

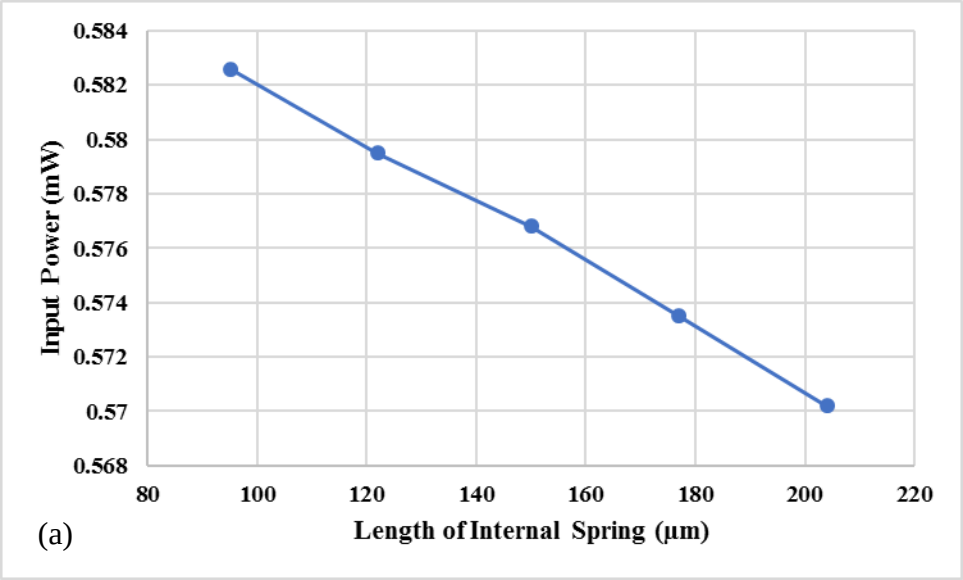

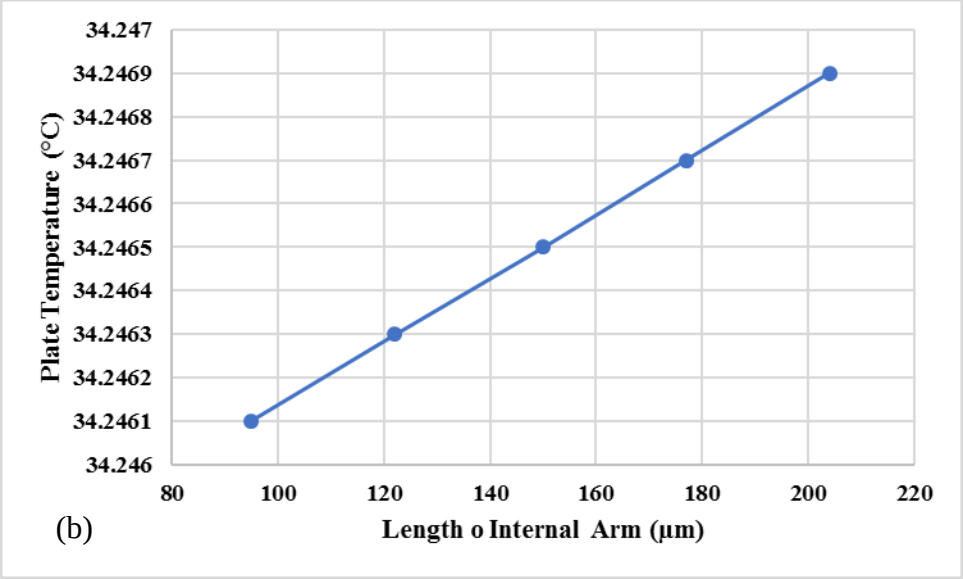

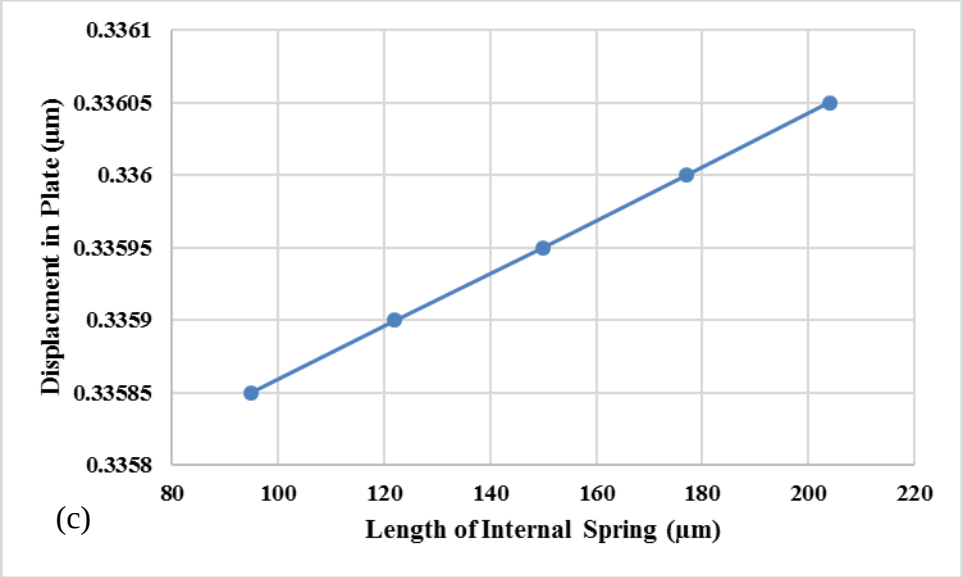

Figure 4.6: (a) LIS varying with PT. (b) LIS varying with IP. (c) LIS varying with DP.

4.2.6 Effect of Width of Thin Arm

Parametric Analysis generated the design curved varying the width of the Curved shape External arms to check its effect on the three outcomes. It is observed from the data range of the Output responses with figures 4.7(a), (b) and (c) that the best results could be gained when the

Length of external arm reaches at the value of 3µm. In order to make the geometry optimized the trends show WTA to have minimum value.

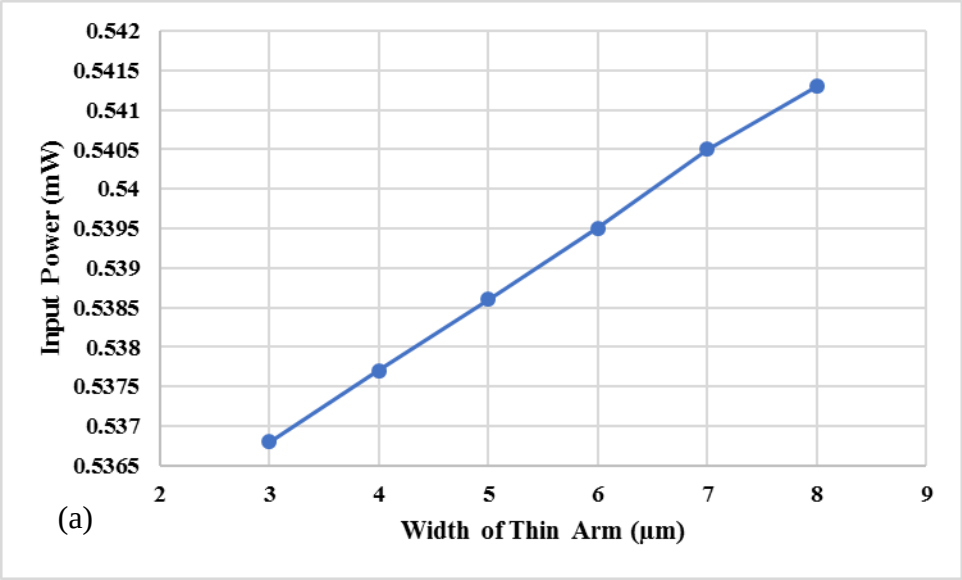

(a)

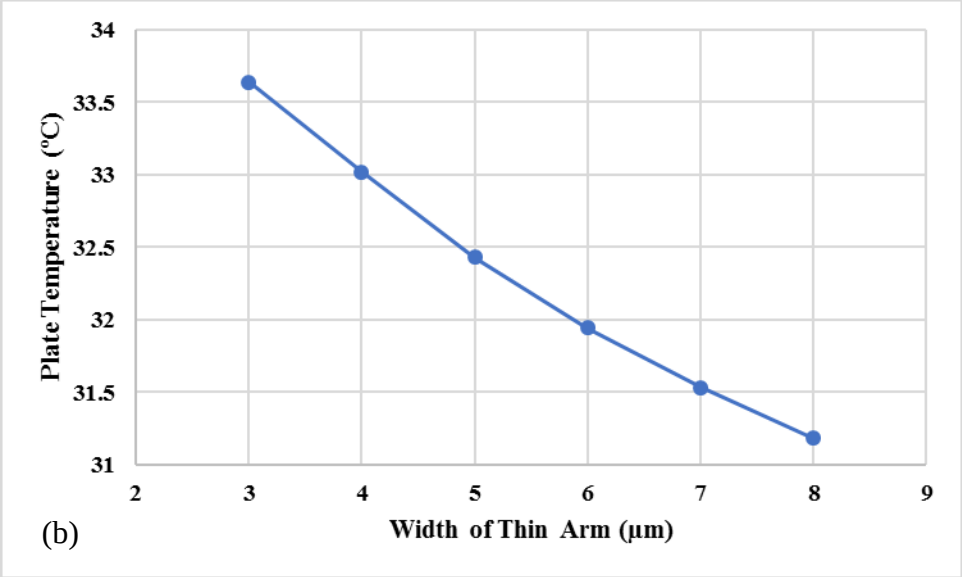

(b)

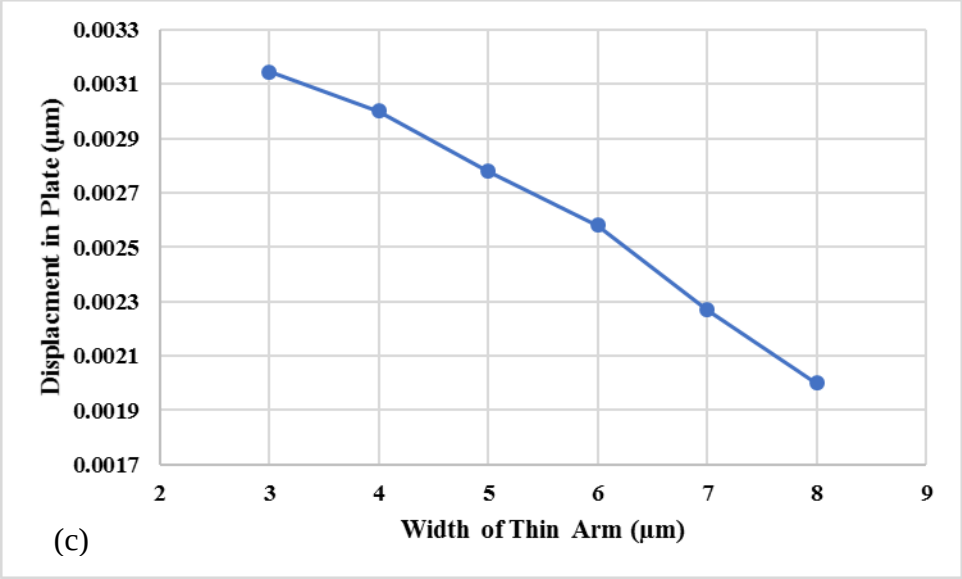

Figure 4.7: (a) WTA varying with PT. (b) WTA varying with IP. (c) WTA varying with DP.

4.2.7 Effect of Length of External Flexure

The design curved varying the length of the External Flexure of the External to check its effect on the three outcomes were observed. It is observed that at the value of 78 µm from the data range of the Output responses the best results were gained. In order to make the geometry optimized the trends show LEF to have maximum value as observed from figure 4.8 (a), (b) and (c).

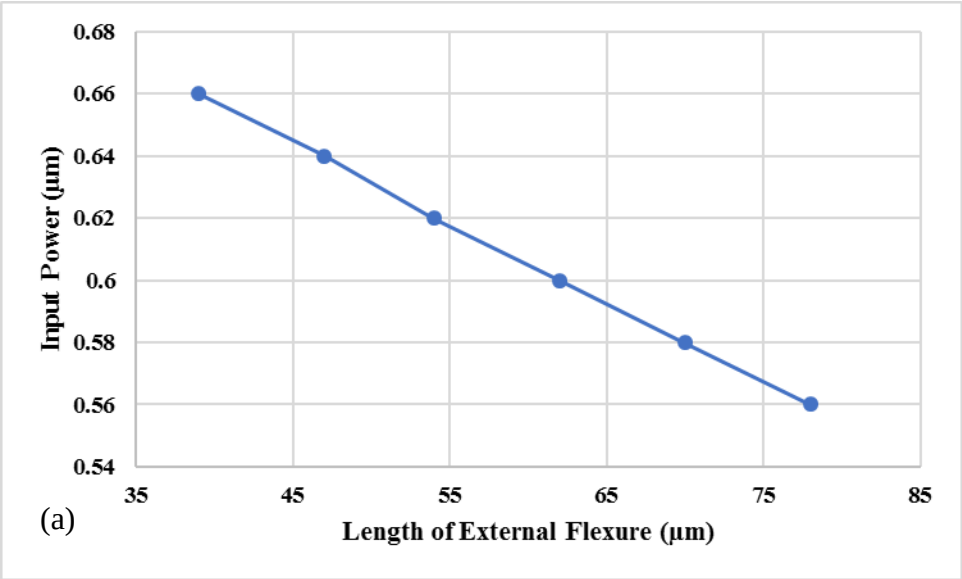

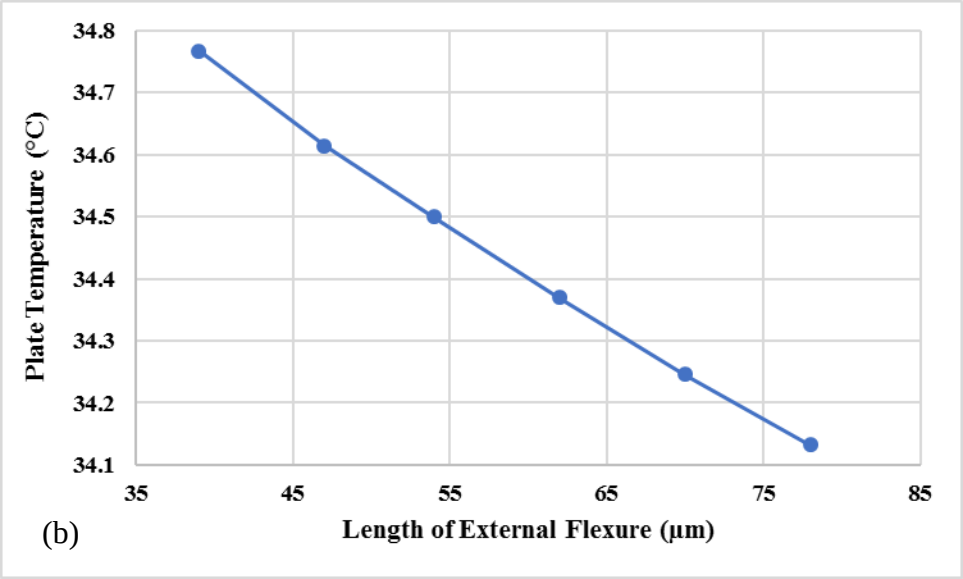

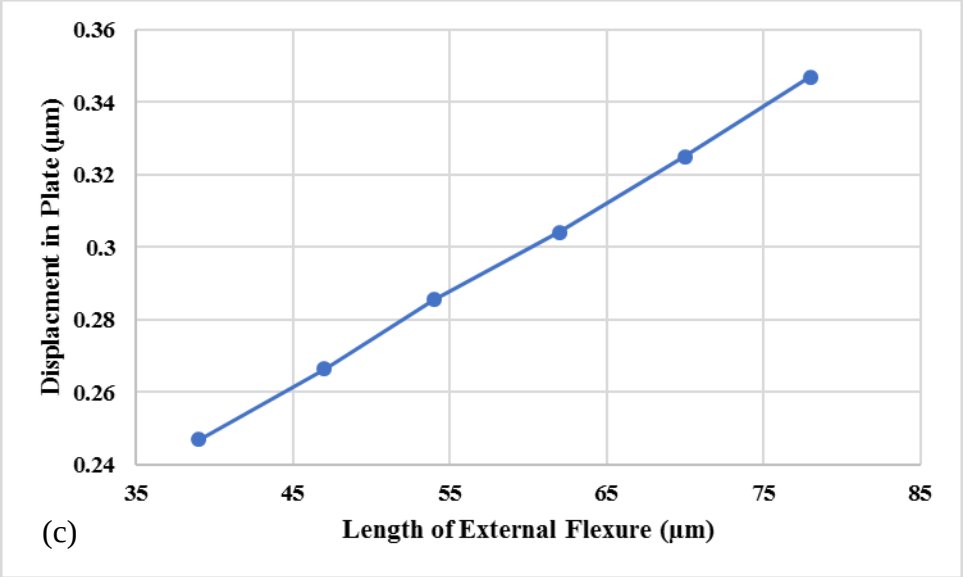

Figure 4.8: (a) LEF varying with PT. (b) LEF varying with IP. (c) LEF varying with DP.

4.2.8 Effect of Length of Internal Flexure

The Length of Internal Arm varying behaviour trend was observed with the desirable outcomes. It is observed that at the value of 61µm from the data range of the Output responses the best results were gained. As observed from figure 4.9 (a), (b) and (c), in order to make the geometry optimized the trends show LIS to have maximum value.

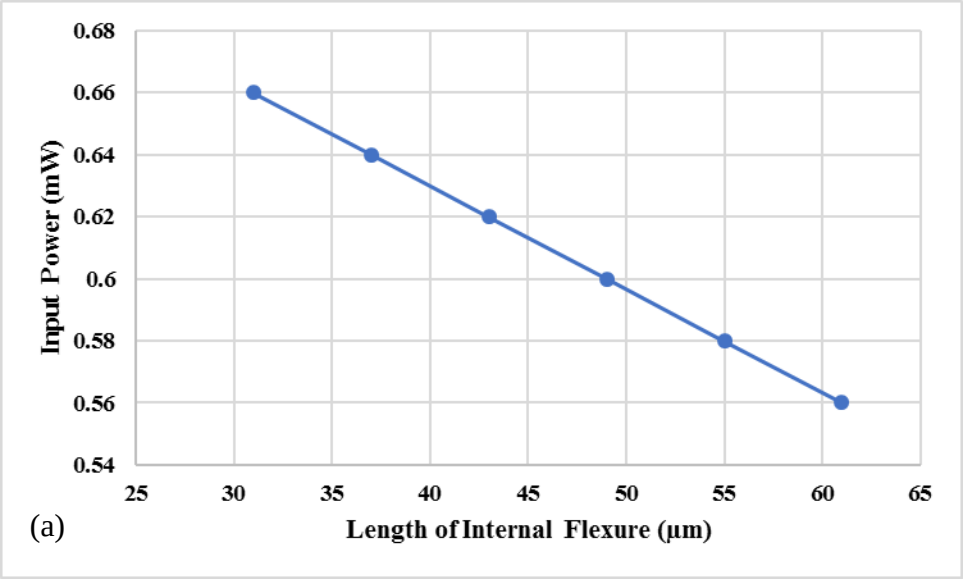
0.68
0.66
0.64
0.62
0.6
0.58
0.56
0.54
Input Power (mW)
25
30
35
40
45
50
55
60
65
Length of Internal Flexure (µm)

(a)

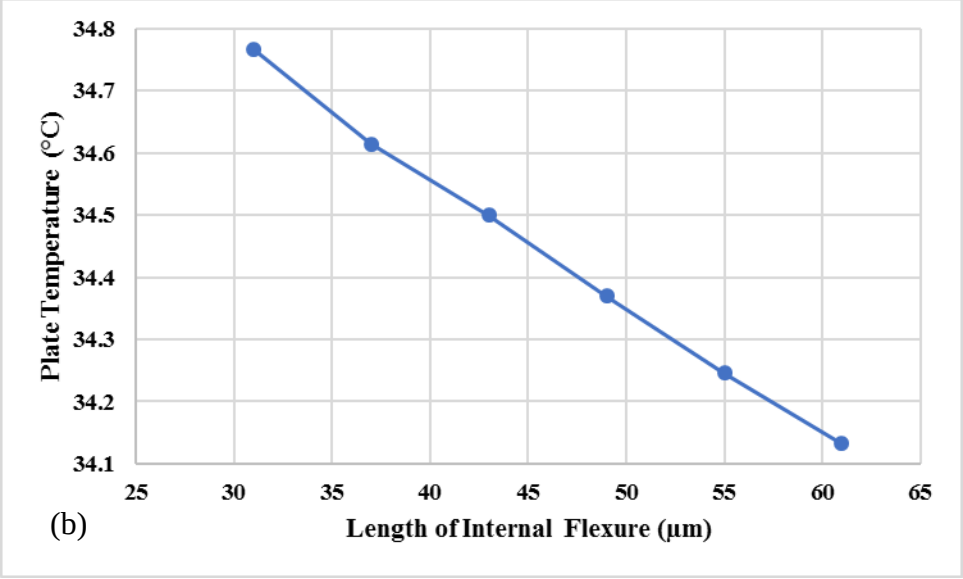
34.8
34.7
34.6
34.5
34.4
34.3
34.2
34.1
Plate Temperature (°C)
25
30
35
40
45
50
55
60
65
Length of Internal Flexure (µm)

(b)

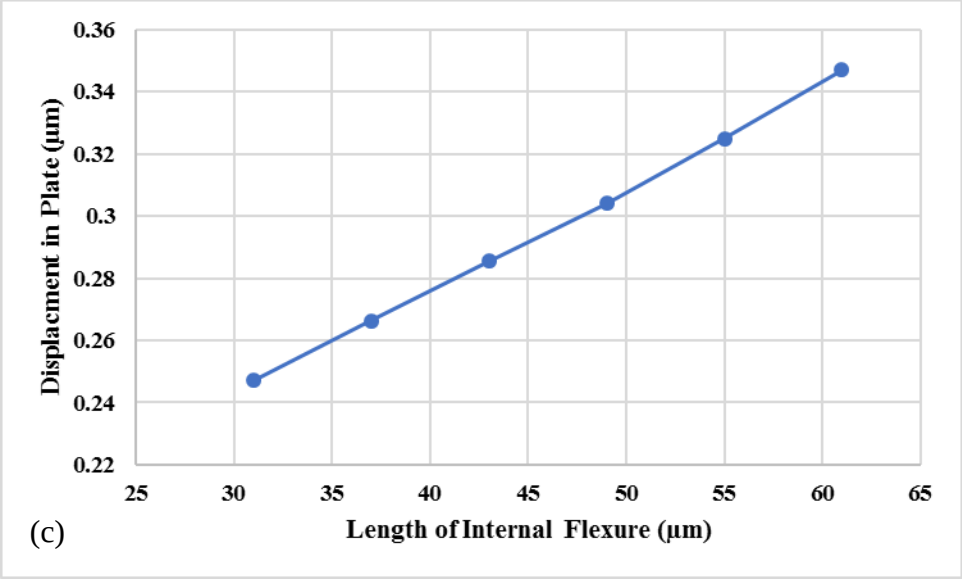

Figure 4.9: (a) LIF varying with PT. (b) LIF varying with IP. (c) LIF varying with DP.

We can observe that the desirable maximized value for Displacement in Plate is more sensitive towards Length of Wide Arms (LEA, LIA), Length of Springs (LES, LIS) So, in order to improve geometry results we need to increase LEA& LIA and increase LES & LIS. Other than that, if we need to decrease the Temperature on Plate along with Input power, then LEF and LIF should be increased to maximum value.

4.3 Verification of Optimized Design

The predicted output responses are further confirmed using FEM based simulation with predicted levels of design variables. The output responses obtained from FEM simulations are deflection 0.5971 µm, at input power of 1.08 mW and a mirror temperature rise of less than 20 Kelvin from ambient. The displacement plot for optimized design is shown in figure 5. The geometry is well justifying our required outcomes.

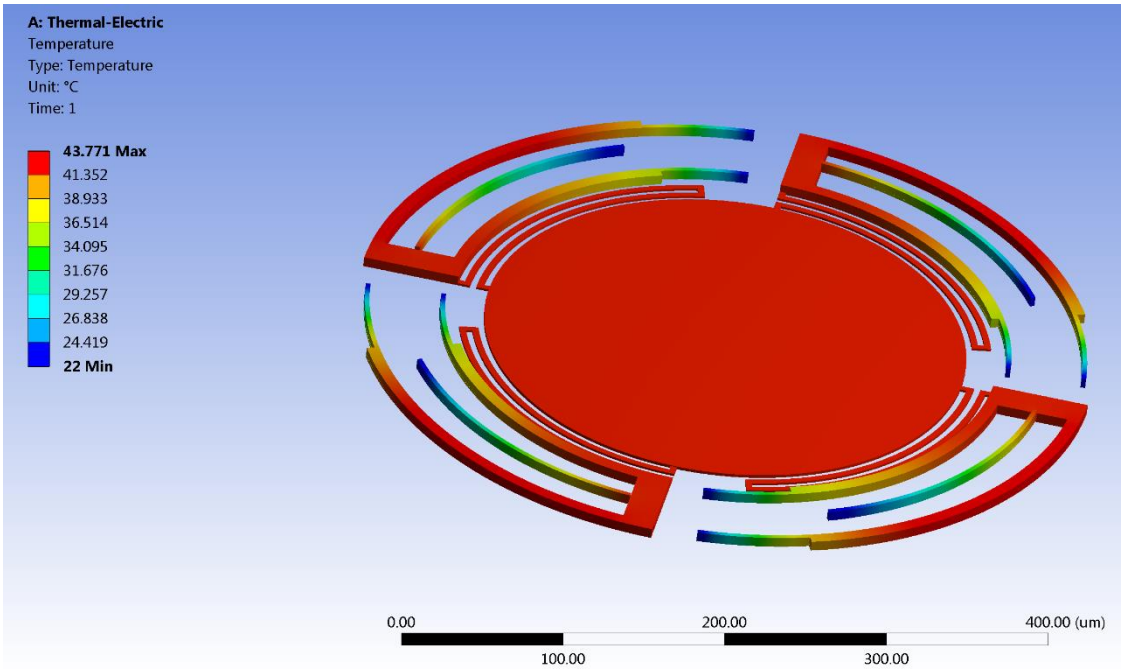

Figure 4.10: Temperature Profile of Optimized device.

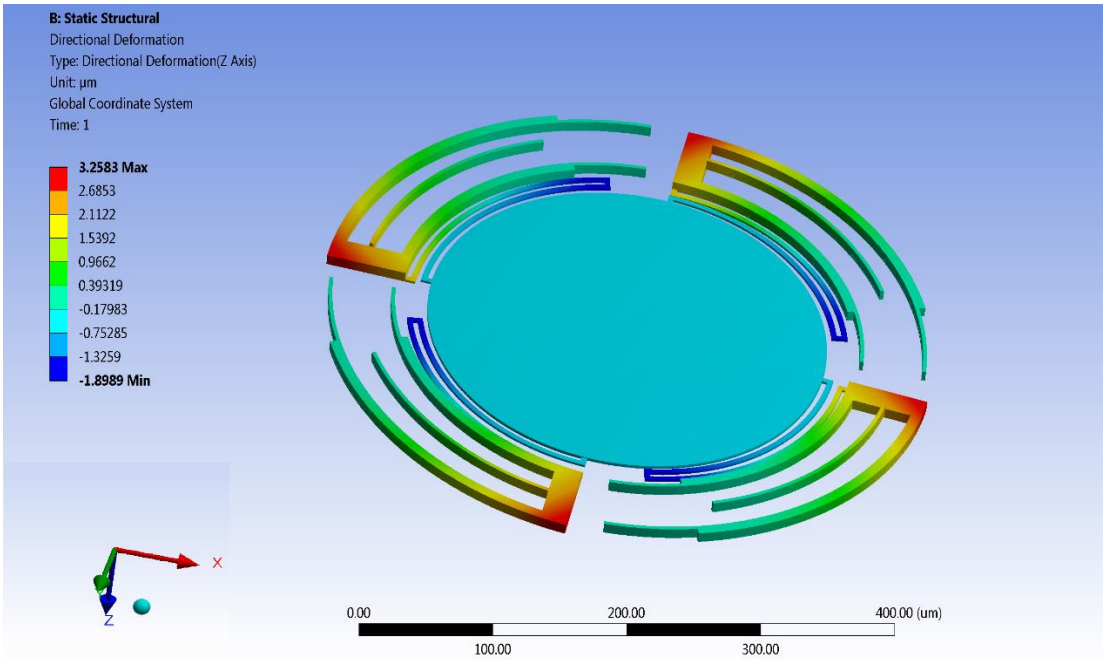

Figure 4.11: Out of plane displacement of Optimized device.

The graph of input power at different temperatures and applied voltage are shown in figure 4.12 and figure 4.13.

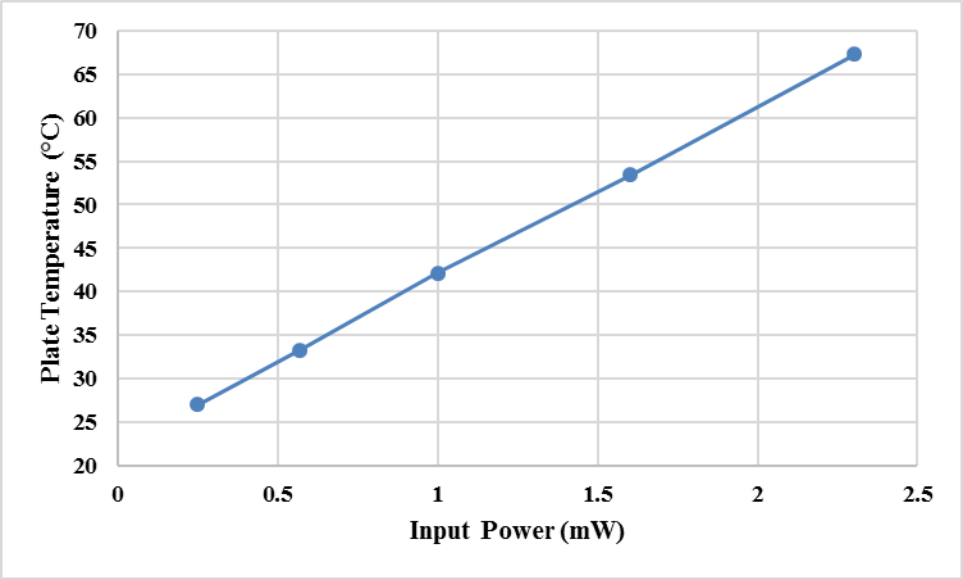

Figure 4.12: Input power Vs plate temperature of optimized device.

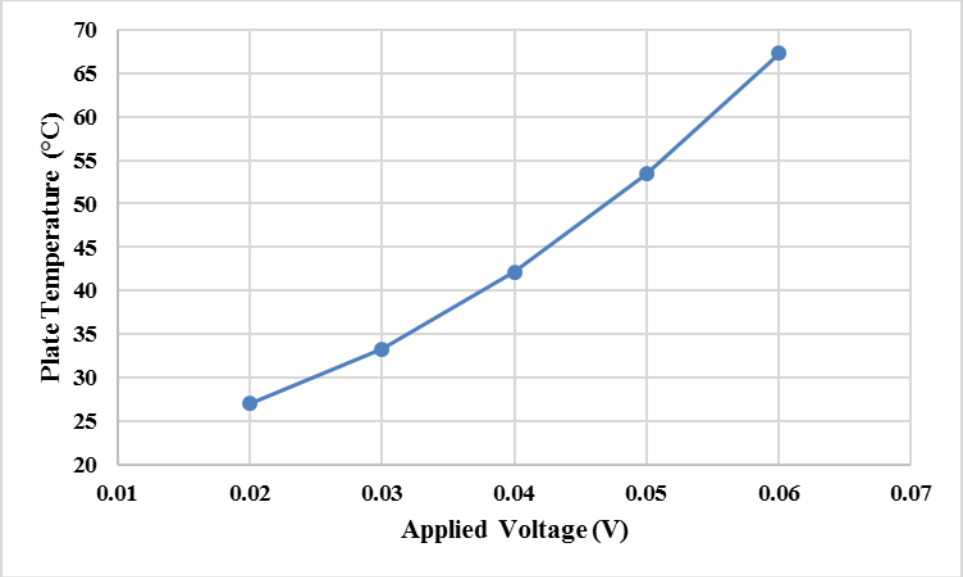

Figure 4.13: Applied voltage Vs plate temperature of optimized device.

The graph of input power at different displacements and applied voltage are shown in figure 4.14 and figure 4.15.

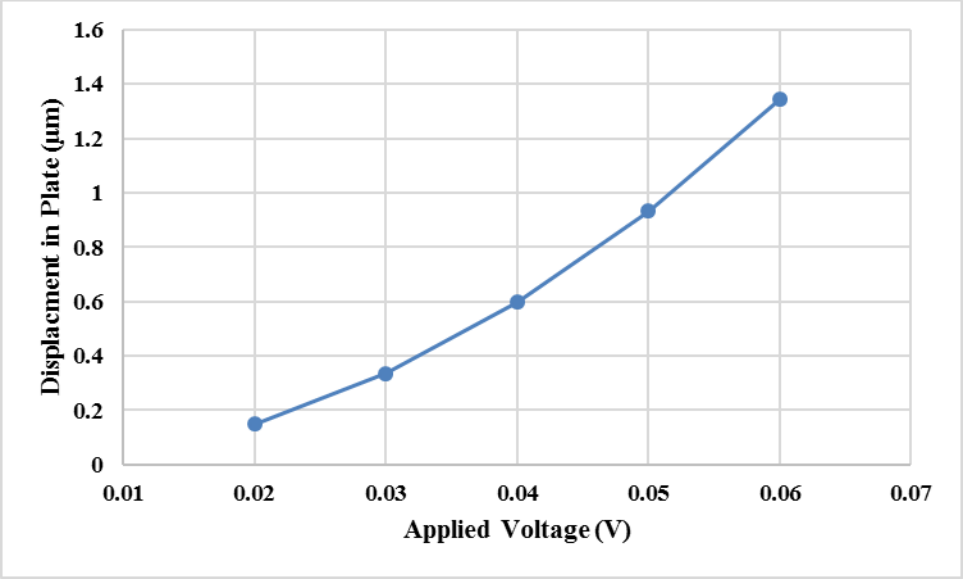

Figure 4.14: Applied voltage Vs displacement.

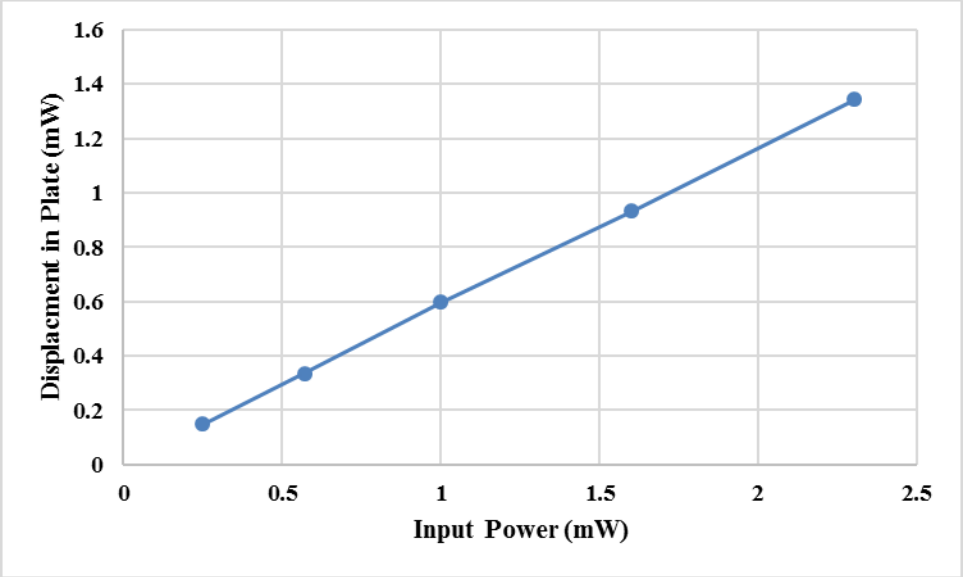

Figure 4.15: Input power Vs displacement.

Chapter 5: Conclusion

In this dissertation, the design and optimization of electrothermally actuated micromirror for Optical Coherence Tomography is presented. Electrothermal actuators are consisting of one structural layer of gold along with SU-8 layer. The voltage applied due to different coefficient of thermal expansion results into expansion and contraction of structural layers. The actuators are connected to mirror plate with flexural springs to achieve maximum deflection angle of mirror plate. Gold is used as the base structural layer for mirror plate which enhance the reflectivity of mirror. The comparison between curved and rectangular geometry is observed, which resulted in choosing curved topology. Optimization of device is done using parametric analysis techniques for design variables. First, design parameters and responses are selected FEM based simulations are done on ANSYS workbench to analyse the output response at different values of design parameters. After observing the significant design variables affecting the output response, tends of behavioural curves is used to investigate the effect of all design variables on output response. Finally, an optimized design is reported on the basis of maximum deflection angle at minimum input power. The device is capable of rotation in two axes as well as out of plane displacement in piston mode deflection. A displacement of 0.5971 μm is achieved at input power of 1.08 mW with applied voltage of 0.04 volt. An out of plane displacement of 5μm is achieved for mirror plate in piston mode for maximum endured temperature on the plate at 1.1 V.

References

[1] Proll, K.P., Nivet, J.M., Körner, K. and Tiziani, H.J., 2003. Microscopic three-dimensional topometry with ferroelectric liquid-crystal-on-silicon displays. Applied optics, 42(10), pp.1773-1778.

[2] Yalcinkaya, A.D., Ergeneman, O. and Urey, H., 2007. Polymer magnetic scanners for bar code applications. Sensors and Actuators A: Physical, 135(1), pp.236-243.

[3] Greenspun, J.T. and Pister, K.S., 2017, June. Low voltage actuation of high force electrostatic latches. In 2017 19th International Conference on Solid-State Sensors, Actuators and Microsystems (TRANSDUCERS) (pp. 898-901). IEEE.

[4] Ren, T.L., Xu, Y., Liu, L.T. and Li, Z.J., 2002. A novel miniature optical switch array with cantilever micromirrors driven by PZT films. Integrated Ferroelectrics, 49(1), pp.193-202.

[5] Bishop, D.J., Giles, C.R. and Austin, G.P., 2002. The Lucent LambdaRouter: MEMS technology of the future here today. IEEE Communications magazine, 40(3), pp.75-79.

[6] Goldberg, H., Yu, D., Speller, K. and Reichert, B., 2002. A MEMS mirror for optical scanning. TECHNICAL PAPERS-SOCIETY OF MANUFACTURING ENGINEERS-ALL SERIES-.

[7] Ahn, S.H. and Kim, Y.K., 2004. Silicon scanning mirror of two DOF with compensation current routing. Journal of Micromechanics and Microengineering, 14(11), p.1455.

[8] Yang, H.A., Tang, T.L., Lee, S.T. and Fang, W., 2007. A novel coilless scanning mirror using eddy current Lorentz force and magnetostatic force. Journal of microelectromechanical systems, 16(3), pp.511-520.

[9] Yalcinkaya, A.D., Urey, H. and Holmstrom, S., 2007. NiFe plated biaxial MEMS scanner for 2-D imaging. IEEE Photonics Technology Letters, 19(5), pp.330-332.

[10] Kim, K.H., Park, B.H., Maguluri, G.N., Lee, T.W., Rogomentich, F.J., Bancu, M.G., Bouma, B.E., de Boer, J.F. and Bernstein, J.J., 2007. Two-axis magnetically-driven MEMS scanning catheter for endoscopic high-speed optical coherence tomography. Optics express, 15(26), pp.18130-18140.

[11] Judy, J.W. and Muller, R.S., 1997. Magnetically actuated, addressable microstructures. Journal of Microelectromechanical systems, 6(3), pp.249-256.

[12] Cho, I.J. and Yoon, E., 2009. A low-voltage three-axis electromagnetically actuated micromirror for fine alignment among optical devices. Journal of Micromechanics and Microengineering, 19(8), p.085007.

[13] Kim, S.J., Cho, Y.H., Nam, H.J. and Bu, J.U., 2008. Piezoelectrically pushed rotational micromirrors using detached PZT actuators for wide-angle optical switch applications. Journal of Micromechanics and Microengineering, 18(12), p.125022.

[14] Koh, K.H., Kobayashi, T., Xie, J., Yu, A. and Lee, C., 2011. Novel piezoelectric actuation mechanism for a gimbal-less mirror in 2D raster scanning applications. Journal of Micromechanics and Microengineering, 21(7), p.075001.

[15] Patterson, P.R., Hah, D., Nguyen, H., Toshiyoshi, H., Chao, R.M. and Wu, M.C., 2002, January. A scanning micromirror with angular comb drive actuation. In Technical Digest. MEMS 2002 IEEE International Conference. Fifteenth IEEE International Conference on Micro Electro Mechanical Systems (Cat. No. 02CH37266) (pp. 544-547). IEEE.

[16] Xie, H., Pan, Y. and Fedder, G.K., 2003. A CMOS-MEMS mirror with curled-hinge comb drives. Journal of Microelectromechanical Systems, 12(4), pp.450-457.

[17] J. Singh, A. Agarwal, and M. Soundarapandian, *A novel electrostatic microactuator for large deflections in MEMS applications*. 2006, pp. 64-68.

[18] H. Xie, J. Sun, L. J. P. o. t. E. M. Wu, and S. O. C. T. o. I. O. a Flexible Printed Circuit Board Permit Fast, "Optical micro-endoscopes for 3D in-vivo imaging," 2010.

[19] Bühler, J., Funk, J., Paul, O., Steiner, F.P. and Baltes, H., 1995. Thermally actuated CMOS micromirrors. Sensors and Actuators A: Physical, 47(1-3), pp.572-575.

[20] Pengwang, E., Rabenorosoa, K., Rakotondrabe, M. and Andreff, N., 2016. Scanning micromirror platform based on MEMS technology for medical application. Micromachines, 7(2), p.24.

[21] Xie, T., Xie, H., Fedder, G.K. and Pan, Y., 2003. Endoscopic optical coherence tomography with a modified microelectromechanical systems mirror for detection of bladder cancers. Applied optics, 42(31), pp.6422-6426.

[22] Jain, A. and Xie, H., 2006. A single-crystal silicon micromirror for large bi-directional 2D scanning applications. Sensors and Actuators A: Physical, 130, pp.454-460. [23] Singh, J., Teo, J.H.S., Xu, Y., Premachandran, C.S., Chen, N., Kotlanka, R., Olivo, M. and Sheppard, C.J.R., 2007. A two axes scanning SOI MEMS micromirror for endoscopic bioimaging. Journal of Micromechanics and Microengineering, 18(2), p.025001.

[24] Yang, J.P., Deng, X.C. and Chong, T.C., 2005. An electro-thermal bimorph-based microactuator for precise track-positioning of optical disk drives. Journal of Micromechanics and Microengineering, 15(5), p.958.

[25] Ataka, M., Omodaka, A., Takeshima, N. and Fujita, H., 1993. Fabrication and operation of polyimide bimorph actuators for a ciliary motion system. Journal of Microelectromechanical Systems, 2(4), pp.146-150..

[26] Izhar, U., Izhar, A.B. and Tatic-Lucic, S., 2011. A multi-axis electrothermal micromirror for a miniaturized OCT system. Sensors and Actuators A: Physical, 167(2), pp.152-161.

[27] Ali, A., Azim, R.A., Khan, U.S., Syed, A.A. and Izhar, U., 2012. Design, simulation and optimization of electrothermal micro actuator. In Applied Mechanics and Materials (Vol. 229, pp. 1939-1943). Trans Tech Publications.

[28] Zhang, X., Duan, C., Liu, L., Li, X. and Xie, H., 2015. A non-resonant fiber scanner based on an electrothermally-actuated MEMS stage. Sensors and Actuators A: Physical, 233, pp.239-245.

[29] Xu, Q., 2015. Design, fabrication, and testing of an MEMS microgripper with dual-axis force sensor. IEEE Sensors Journal, 15(10), pp.6017-6026.

[30] Andersen, K.N., Carlson, K., Petersen, D.H., Mølhave, K., Eichhorn, V., Fatikow, S. and Bøggild, P., 2008. Electrothermal microgrippers for pick-and-place operations. Microelectronic engineering, 85(5-6), pp.1128-1130..

[31] Khazaai, J.J., Qu, H., Shillor, M. and Smith, L., 2011, October. Design and fabrication of electro-thermally activated micro gripper with large tip opening and holding force. In SENSORS, 2011 IEEE (pp. 1445-1448). IEEE.

[32] Chen, D. S., Yin, C. Y., Lai, R. J., & Tsai, J. C. (2009, January). A multiple degrees of freedom electrothermal actuator for a versatile MEMS gripper. In Micro Electro Mechanical Systems, 2009. MEMS 2009. IEEE 22nd International Conference on (pp. 1035-1038). IEEE.

[33] Colinjivadi, K. S., Lee, J. B., & Draper, R. (2008). Viable cell handling with high aspect ratio polymer chopstick gripper mounted on a nano precision manipulator. Microsystem Technologies, 14(9-11), 1627-1633.

[34] Mata, A., Fleischman, A. J., & Roy, S. (2006). Fabrication of multi-layer SU-8 microstructures. Journal of micromechanics and microengineering, 16(2), 276.

[35] Voicu, R., Tibeica, C., & Muller, R. (2009, April). Design and simulation study for an electro-thermally actuated micromanipulator. In Thermal, Mechanical and Multi-Physics simulation and Experiments in Microelectronics and Microsystems, 2009. EuroSimE 2009. 10th International Conference on (pp. 1-5). IEEE.

[36] D. Huang *et al.*, "Optical coherence tomography," (in eng), *Science*, vol. 254, no. 5035, pp. 1178-81, Nov 22 1991.

[37] Park, S., Chung, S.R. and Yeow, J.T., 2008. A design analysis of micromirrors in stacked configurations with moving electrodes. Int. J. Smart Sens. Intell. Syst, 1(2), pp.480-497

[38] Ogando, K., La Forgia, N., Zarate, J.J. and Pastoriza, H., 2012. Design and characterization of a fully compliant out-of-plane thermal actuator. Sensors and Actuators A: Physical, 183, pp.95-100.

[39] Kim, Y.S., Dagalakis, N.G. and Gupta, S.K., 2012. Design, fabrication and characterization of a single-layer out-of-plane electrothermal actuator for SOI-MEMS applications.

[40] Kim, Y.S., Dagalakis, N.G. and Gupta, S.K., 2013. Creating large out-of-plane displacement electrothermal motion stage by incorporating beams with step features. Journal of Micromechanics and Microengineering, 23(5), p.055008.

[41] Venditti, R., Lee, J.S., Sun, Y. and Li, D., 2006. An in-plane, bi-directional electrothermal MEMS actuator. Journal of Micromechanics and Microengineering, 16(10), p.2067.

[42] Peng, Wuyong, Zhixiong Xiao, and K. R. Farmer. "Optimization of thermally actuated bimorph cantilevers for maximum deflection." Nanotech Proceedings 1 (2003): 376-379.

[43] Liu, L., Pal, S. and Xie, H., 2012. MEMS mirrors based on a curved concentric electrothermal actuator. Sensors and Actuators A: Physical, 188, pp.349-358..

[44] Premachandran, C.S., Khairyanto, A., Chen, K., Singh, J., Wang, S.X., Yingshun, X., Nanguang, C., Sheppard, C.J.R., Olivo, M. and Lau, J., 2008, May. Influence of optical probe packaging on a 3D MEMS scanning micro-mirror for optical coherence tomography (OCT) applications. In 2008 58th Electronic Components and Technology Conference (pp. 829-833). IEEE.

[45] Liu, W. and Talghader, J.J., 2003. Current-controlled curvature of coated micromirrors. Optics letters, 28(11), pp.932-934.

[46] Liu, A.Q., 2008. Photonic MEMS devices: design, fabrication and control. CRC press..

[47] Liu, R., Wang, H., Li, X., Tang, J., Mao, S. and Ding, G., 2008. Analysis, simulation and fabrication of MEMS springs for a micro-tensile system. Journal of Micromechanics and Microengineering, 19(1), p.015027..

Completion Certificate

It is certified that the contents of thesis document titled "***Multi-Response Design Optimization of Two Axes SU-8 based Scanning Micromirror for Endoscopic Imaging***" submitted by NS Fizza Javaid, Registration No. 00000170885 have been found satisfactory in all respects as per the requirements of Main Office, NUST (Exam branch).

Supervisor: _____

Dr. Muhammad Mubasher Saleem

Date: ____ August, 2019